



Wflow_sbm v0.6.1, a spatially distributed hydrologic model: from global data to local applications

Willem J. van Verseveld¹, Albrecht H. Weerts^{1,2}, Martijn Visser¹, Joost Buitink¹, Ruben O. Imhoff^{1,2}, H el ene Boisgontier¹, Laur ene Bouaziz¹, Dirk Eilander^{1,3}, Mark Hegnauer¹, Corine ten Velden¹, and Bobby Russell¹

¹Department of Inland Water Systems, Deltares, P.O. Box 177, 2600MH Delft, The Netherlands

²Hydrology and Quantitative Water Management Group, Department of Environmental Sciences, Wageningen University & Research, P.O. BOX 47, 6700 AA Wageningen, The Netherlands

³Institute for Environmental Studies (IVM), Vrije Universiteit Amsterdam, Amsterdam, the Netherlands

Correspondence: Willem van Verseveld (willem.vanverseveld@deltares.nl)

Abstract. The wflow_sbm hydrologic model, recently released by Deltares, as part of the Wflow.jl (v0.6.1) modelling framework is being used to better understand and potentially address multiple operational and water resources planning challenges from catchment scale, national scale to continental and global scale. Wflow.jl is a free and open-source distributed hydrologic modelling framework written in the Julia programming language. The development of wflow_sbm, the model structure, equations and functionalities are described in detail, including example applications of wflow_sbm. The wflow_sbm model aims to strike a balance between low-resolution, low-complexity and high-resolution, high-complexity hydrologic models. Most wflow_sbm parameters are based on physical characteristics or processes and at the same time wflow_sbm has a runtime performance well suited for large-scale high-resolution model applications. Wflow_sbm models can be set a priori for any catchment with the Python tool HydroMT-Wflow based on globally available datasets and through the use of point-scale (pedo)transfer functions and suitable upscaling rules and generally results in a satisfactory ($0.4 \geq$ Kling-Gupta Efficiency (KGE) < 0.7) to good ($KGE \geq 0.7$) performance a-priori (without further tuning). Wflow_sbm includes relevant hydrologic processes as glacier and snow processes, evapotranspiration processes, unsaturated zone dynamics, (shallow) groundwater and surface flow routing including lakes and reservoirs. Further planned developments include improvements on the computational efficiency and flexibility of the routing scheme, implementation of a water demand and allocation module for water resources modelling, the addition of a deep groundwater concept and distributed computing with a focus on multi-node parallelism.

1 Introduction

Hydrologic models have proven to be useful tools in better understanding multiple operational and water resources planning challenges including drought (e.g., Trambauer et al., 2015) and flood forecasting (e.g., Alfieri et al., 2013), the assessment of water availability (e.g., van Beek et al., 2011) and to analyse the impact of food production on river systems (e.g., J agermeyr et al., 2017). An advantage of spatially distributed (gridded) hydrologic models, in contrast to spatially lumped models, is the ability to directly use the spatially varying information contained in spatial datasets for model setup, forcing and validation.



High resolution spatial datasets become increasingly available, often at a global scale, and can be used to represent land cover, vegetation (e.g. Leaf Area Index) and soil properties in spatially distributed hydrologic models. For example, SoilGrids provides gridded soil information at 250 m resolution globally (Hengl et al., 2017). With regard to forcing, the release of the fifth generation ECMWF atmospheric reanalysis of the global climate (ERA5) (Hersbach et al., 2020) dataset (1959-present) is worth mentioning, with a spatial resolution of $\sim 31 \text{ km} \times 31 \text{ km}$ and a temporal resolution of 1 hour, and ERA5 Land with a spatial resolution of $\sim 9 \text{ km} \times 9 \text{ km}$. Recently, it has been argued that the development of a hyperresolution global hydrological model at 1 km^2 or finer is a “grand challenge for hydrology” and is needed to address the water problems facing society (Wood et al., 2011; Bierkens et al., 2014).

Notwithstanding the advantages of and need for (hyperresolution) spatially distributed hydrologic models, parameterization of these models is not straightforward, because of overparameterization and as a result overfitting (Jakeman and Hornberger, 1993; Beven, 1993, 2006). Furthermore, transferability of hydrologic parameters across spatial and temporal scales is important for reducing calibration time and the application of hydrologic models in ungauged or poorly gauged basins. However the impact of transferring model parameters across spatial and temporal resolutions on model performance is unequivocal and high parameter transferability across spatial resolution may also be the result of inadequate representation of spatial variability in (large-scale) hydrologic models (Melsen et al., 2016). Finally, there is the scientific debate on the “best” approach to process-based hydrologic modelling leading to appropriate physical realism, especially related to model structure and model solutions (Kirchner, 2006; Clark et al., 2016, 2017).

Concerning hydrologic model structure and solutions, Hrachowitz and Clark (2017) classified hydrologic models along two dimensions, process complexity and spatial resolution. Hydrologic models with high process complexity and spatial resolution are for example PARFLOW (Kollet and Maxwell, 2006), HydroGeoSphere (Brunner and Simmons, 2012) and HYDRUS-3D (Šimůnek et al., 2008), while for example HBV (Bergström, 1992), SUPERFLEX (Fenicia et al., 2011) and FLEX-Topo (Gao et al., 2014) are characterized by low spatial resolution and low process complexity. For the high-resolution, high-complexity hydrologic models the majority of the parameters are based on physical characteristics, and may be directly or by upscaling be estimated from field or remotely sensed observations, depending on the model resolution. For low-resolution, low-complexity hydrologic models, the majority of parameters are effective parameters at the catchment-scale and calibration is required to identify parameter values. Generally, high-resolution, high-complexity hydrologic models are computationally demanding, which limits their application to smaller domains, or requires a reduction in model resolution or high performance computing resources for large-scale applications. Free and open-source spatially distributed hydrologic models that require a low calibration effort (parameters based on physical characteristics) and have fast run times applicable for large-scale high-resolution modelling (medium complexity), are not or very limited available to our knowledge.

Wflow_sbm represents a family of spatially distributed hydrologic models that have the vertical hydrologic simple bucket model (SBM, Vertessy and Elsenbeer, 1999) concept in common, but can have different lateral concepts that control how water is routed for example over the land or river domain. This paper presents the wflow_sbm model configuration that makes use of the kinematic-wave approach for river, overland and lateral subsurface flow. It is part of the open-source distributed hydrologic model platform Wflow.jl (van Verseveld et al., 2022a) developed at Deltares. Wflow_sbm strikes a balance between



low-resolution, low-complexity and high-resolution, high-complexity hydrologic models, giving an answer to most of the
aforementioned challenges. In this model, the soil part is largely based on Topog_SBM (Vertessy and Elsenbeer, 1999), with
gravity-based infiltration and vertical flow through the soil column as well as capillary rise representing a simplified version of
60 the Richards' equation. Furthermore it uses a 1-D kinematic wave approach for channel, overland and lateral subsurface flows
similar to TOPKAPI (Benning, 1994; Todini and Ciarapica, 2002), G2G (Bell et al., 2007), 1K-DHM (Tanaka and Tachikawa,
2015) and Topog_SBM (Vertessy and Elsenbeer, 1999), as an approximation for dynamic waves and variably saturated sub-
surface flow (Richards' equation). The advantage is that most wflow_sbm parameters are based on physical characteristics and
at the same time wflow_sbm has a run time performance well suited for large-scale high-resolution modelling.

65 Furthermore, in line with the need to improve the transparency, reproducibility and ease of setting up hydrologic models
(Clark et al., 2017; Knoben et al., 2021), we use the wflow plugin (HydroMT-Wflow, Eilander et al., 2022) of the HydroMT
Python package (Eilander and Boisgontier, 2022) to set up wflow_sbm models for any catchment based on globally avail-
able datasets, e.g. SoilGrids (Hengl et al., 2017), GlobCover-2009 (Arino et al., 2010) and MERIT Hydro (Yamazaki et al.,
2019). Point scale (pedo)transfer-functions (PTFs) from literature are used to derive model parameters at the highest available
70 resolution of the data and scaled with suitable upscaling operators (Imhoff et al., 2020) to the desired model resolution. The
advantage is that transfer functions are only constrained by field and laboratory measurements, although we acknowledge that
the scale at which these PTFs can be applied remains uncertain (Van Looy et al., 2017; Samaniego et al., 2017). Nevertheless,
the application of this method to the Rhine basin resulted for most gauging stations in the central and northern part of the
basin in Kling-Gupta Efficiency (KGE, Gupta et al., 2009) values between 0.6 and 0.9 (Imhoff et al., 2020). In the meantime,
75 wflow_sbm and the forementioned approach was used and tested to model the basins in the upper region of the greater Chao
Phraya River in Thailand (Wannasin et al., 2021a, b) and the Citarum river in Indonesia (Rusli et al., 2021). Meijer et al.
(2021) used wflow_sbm to rapidly develop a water resources model for the Upper Niger Basin using global online data. Sperna
Weiland et al. (2021) used wflow_sbm to assess climate change impacts in nine river basins across Europe. While Aerts et al.
(2021) used wflow_sbm to assess impact of various model resolutions (200m, 1km, 3km) on wflow_sbm performance for the
80 CAMELS-US dataset.

The objective of this paper is to describe the wflow_sbm model in detail (model structure and equations) and to present
some applications and envisaged future developments. Section 2 describes the development of the wflow_sbm model within
the Wflow.jl framework, its model structure, model equations, and functionalities. In section 3 we describe the computational
performance of wflow_sbm. Several applications of wflow_sbm are demonstrated in section 4, followed by conclusions and
85 foreseen future work in section 5.

2 Model description

2.1 Overview

Wflow.jl (v0.6.1) (van Verseveld et al., 2022a) is an open-source modelling framework for distributed hydrologic modelling,
containing multiple distributed hydrologic model concepts, implemented in the programming language Julia (Bezanson et al.,



90 2017). It is a continuation of the wflow framework (Schellekens et al., 2020) which is based on Python PCRaster (Karssenber
et al., 2010). The switch to the programming language Julia was made because Julia offers high performance (speed of C),
required for large-scale high-resolution hydrologic model applications, and is an “easy-to-use” language. Julia also opens
up opportunities to parallelize the code for further improved computational performance. Wflow.jl provides several different
vertical and lateral concepts that can be used for hydrologic modelling and is Basic Model Interface (BMI) compliant. Three
95 vertical hydrologic concepts are available within Wflow.jl: HBV-96 (wflow_hbv), FLEXTopo (wflow_flextopo) and SBM
(wflow_sbm).

Wflow_sbm is the main hydrologic model concept of the Wflow.jl framework and represents a family of hydrologic models
that have the vertical SBM concept in common. Wflow_sbm can have different lateral concepts that control how water (river,
overland and subsurface flow) is routed, easily enabled by the modular structure of Wflow.jl. The wflow_sbm model presented
100 here (Fig. 1) consists of the vertical SBM concept and for the lateral components the kinematic-wave approach is used for
river, overland and lateral subsurface flow, similar to TOPKAPI (Benning, 1994; Todini and Ciarapica, 2002), G2G (Bell et al.,
2007), 1K-DHM (Tanaka and Tachikawa, 2015) and Topog_SBM (Vertessy and Elsenbeer, 1999). The vertical SBM concept
is largely based on Topog_SBM (Vertessy and Elsenbeer, 1999) that considers the soil as a “bucket” with a saturated and
unsaturated store. While Topog_SBM is specifically designed to simulate fast-runoff processes during discrete storm events
105 in small catchments (< 10 km²) as evapotranspiration losses are ignored, wflow_sbm can be applied to a wider variety of
catchments. The main differences of wflow_sbm with Topog_SBM are:

- The addition of evapotranspiration and interception losses.
- The addition of a root water uptake reduction function (Feddes et al., 1978).
- The addition of capillary rise.
- 110 – The addition of glacier, snow build-up and melting processes and an avalanche option for downhill snow transport.
- Water is routed downstream over an eight direction (D8) network, instead of the element network based on contour lines
and trajectories, used by Topog_SBM.
- The option to divide the soil column into different layers, to allow for transfer of water within the unsaturated zone.

Wflow_sbm has been applied in various catchments around the world showing satisfactory ($0.4 \geq KGE < 0.7$) to good (KGE
115 ≥ 0.7) performance (e.g., López López et al., 2016; Hassaballah et al., 2017; Giardino et al., 2019; Gebremicael et al., 2019;
Imhoff et al., 2020; Laverde-Barajas et al., 2020; Wannasin et al., 2021a, b; Rusli et al., 2021; Meijer et al., 2021).

Figure 1 presents the different processes and fluxes in the wflow_sbm model. Precipitation enters each grid cell through the
interception routine (total precipitation is first intercepted), based on the Gash model (Gash, 1979) or a modified Rutter model
(Rutter et al., 1971, 1975), depending on the time stamp the model is using. Throughfall and stemflow from the interception
120 routine are transferred to the optional snow (based on the HBV-96 hydrologic model concept (Bergström, 1992)) and glacier
routines (based on the HBV-light degree-day based model (Seibert et al., 2018)). The soil in every grid cell is considered as



a single bucket, divided into a saturated and unsaturated store, with the option to divide the soil column into different layers. Available infiltration (stemflow and throughfall not converted to snow, including meltwater) infiltrates into the soil or becomes direct runoff based on the river fraction or open water (excluding rivers) fraction. Soil infiltration is determined separately for the paved and nonpaved areas, as these have different infiltration capacities. Naturally, only the water that can be stored in the soil can infiltrate. If not all water can infiltrate, this is added as saturation excess water to the runoff routing scheme for overland flow. Infiltration excess occurs when the infiltration capacity is smaller than the available infiltration rate, and this amount of water is also added to the runoff routing scheme for overland flow. An exponential decay of the saturated hydraulic conductivity with soil depth is assumed. Transfer of water in the unsaturated store, and to the saturated store is based on Brooks and Corey (1964) when the soil column is divided into different layers, and in case of one soil layer also the original Topog_SBM vertical transfer formulation can be used. Part of the water evaporates through soil evaporation, transpiration which is first derived from the saturated store if roots intersect with the saturated store and then from the unsaturated store, and open water (excluding rivers) and river evaporation. Besides transpiration, capillary rise and leakage result in a flux from the saturated store, to the unsaturated store and outside of the model domain, respectively. The kinematic-wave approach is used to route subsurface flow laterally. Saturation excess water when the water table of lateral subsurface flow reaches the surface, and exfiltration of water in the unsaturated store to the surface because of a changing water table, is added as saturation excess water to the runoff routing scheme for overland flow. Also for overland and river the kinematic-wave approach is used. Reservoir and lake models (optional) can be included within the kinematic wave river routing.

The wflow_sbm model is described in more detail, including equations, in sections 2.2 - 2.7. These sections link to the main routines of wflow_sbm (Fig. 1):

1. Interception (section 2.2)
2. Snow and glaciers (section 2.3)
3. Soil module and evapotranspiration (section 2.4)
4. Lateral subsurface flow (section 2.5)
5. Surface routing (section 2.6)
6. Reservoirs and lakes (section 2.7)

Table A1 lists wflow_sbm state and flux variables (non-exhaustive). Additionally, wflow_sbm model inputs and parameters are listed in Table A2, including default values. Table A1 and A2 both list the symbols that are used in sections 2.2 - 2.7 as well as the corresponding Wflow.jl names.

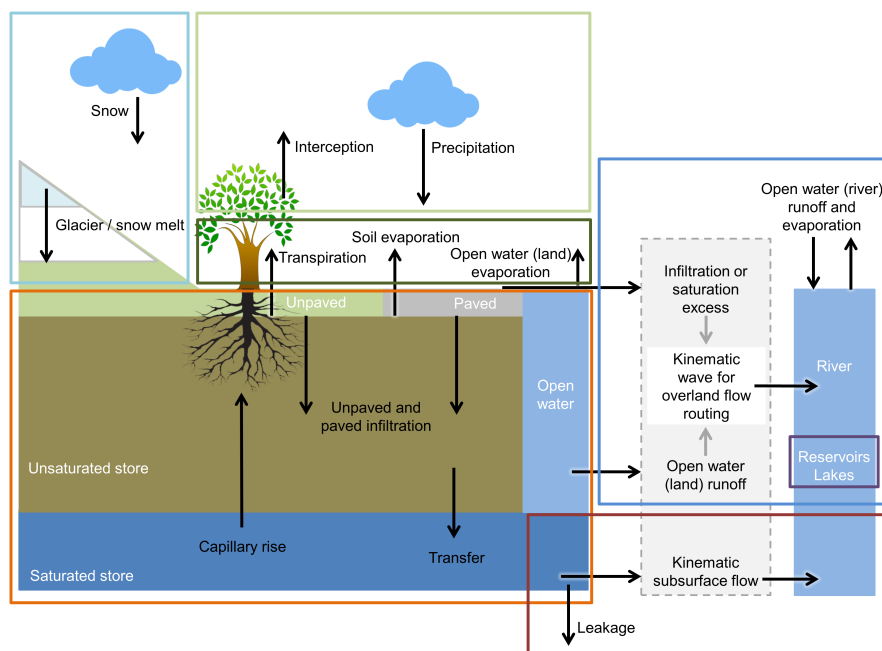


Figure 1. An overview of the different processes and fluxes in the wflow_sbm model (adopted from van Verseveld et al., 2022a). The model includes the following routines: Interception (green, section 2.2), Snow and glaciers (light blue, section 2.3), Soil module and evapotranspiration (orange, section 2.4), Lateral subsurface flow (brown, section 2.5), Surface routing (dark blue, section 2.6) and Reservoirs and lakes (black, section 2.7).

150 To run a wflow_sbm model several files are required: 1) a configuration file in the Tom's Obvious, Minimal Language (TOML) format, 2) a NetCDF file containing static and (optional) cyclic data, for example model parameters, flow direction, river network and gauges, and 3) a NetCDF file containing forcing data (precipitation, potential evapotranspiration and temperature fields). Storage and rating curves for lakes should be provided in CSV format. The static and forcing maps should have the same spatial domain and resolution, e.g. regridding of forcing data is not supported. The focus of Wflow.jl is on the
155 computations (computational engine), and the modular structure of the code simplifies extending the base code for pre- and post-processing purposes.

In the TOML file the following aspects are defined: simulation period and model time step, model specific settings like the model type (e.g. "sbm" for wflow_sbm) or whether to include snow modelling, locations and names of input and output files, mapping of internal model variables and parameters to external NetCDF variables, optional modification of input model
160 parameters and forcing, and output options. Glacier and snow modelling, and lake and reservoir modelling are optional (specific model settings). Wflow_sbm runs typically at a daily time step (recommended maximum model time step) and a spatial resolution of ~1 km (we recommend a maximum grid resolution of ~5 km). Sub-daily model time steps are supported, for example for flow forecasting purposes or small (fast responding) catchments. Output options consist of gridded data (NetCDF) and scalar data (NetCDF or CSV). Scalar data can be generated for individual grid cells or areas (e.g. sub-catchment).



165 For users that mainly want to run simulations without installing Julia, Wflow.jl is available as a compiled executable (cross platform). Users that want to explore and modify the code, and want to extend Wflow.jl (e.g. writing your own Julia scripts around the Wflow.jl package), we recommend to install Wflow.jl as a Julia package. The Wflow.jl documentation provides more details about the Wflow.jl installation and usage in the “User guide” section (van Verseveld et al., 2022a).

2.2 Interception

170 For interception the Gash model (Gash, 1979) for daily time steps and a modified Rutter model (Rutter et al., 1971, 1975) for sub-daily time steps is available within the Wflow.jl framework. The Gash model is a daily interception model, by assuming one precipitation event per day, and applied when wflow_sbm runs at a daily time step. For sub-daily time steps a modified Rutter model is used.

2.2.1 Gash model

175 The original Gash model considers precipitation input as a series of discrete storm events, where each storm event is divided into three sequential phases: 1) wetting phase during which precipitation saturates the canopy, 2) saturation phase during which the canopy is saturated and the precipitation intensity is higher than the average evaporation rate of the saturated canopy and 3) drying phase during the period after precipitation has ceased. The amount of water needed to completely saturate the canopy ($P_{\text{sat,max}}^t$ [mm]) is defined as:

$$180 \quad P_{\text{sat,max}}^t = \frac{-P_{\text{sat}}^t S_{\text{canopy,max}}}{E_{\text{sat}}^t} \ln \left[1 - \frac{E_{\text{sat}}^t}{P_{\text{sat}}^t} (\max((1 - f_{\text{canopygap}} - f_{\text{stemflow}}), 0))^{-1} \right], \quad (1)$$

where P_{sat}^t [mm t^{-1}] is the average precipitation intensity and E_{sat}^t [mm t^{-1}] is the average evaporation rate during saturation of the canopy, $S_{\text{canopy,max}}$ [mm] is the canopy storage capacity, $f_{\text{canopygap}}$ [-] is the canopy gap fraction and f_{stemflow} [-] is the stemflow fraction. The stemflow fraction f_{stemflow} in wflow_sbm is defined as a fixed fraction (0.1) of the canopy gap fraction $f_{\text{canopygap}}$, and stemflow P_{stemflow}^t [mm] at time step t is calculated as the stemflow fraction of the precipitation amount P^t [mm] at time step t :

$$P_{\text{stemflow}}^t = f_{\text{stemflow}} P^t. \quad (2)$$

Interception during the wetting phase I_{wet}^t [mm], saturation phase I_{sat}^t [mm] and dry phase I_{dry}^t [mm] at time step t are given by Eq. (3) - (5):

$$I_{\text{wet}}^t = \begin{cases} \max((1 - f_{\text{canopygap}} - f_{\text{stemflow}}), 0) P_{\text{sat,max}}^t - S_{\text{canopy,max}}, & \text{if } P^t > P_{\text{sat,max}}^t \\ \max((1 - f_{\text{canopygap}} - f_{\text{stemflow}}), 0) P^t, & \text{otherwise} \end{cases} \quad (3)$$



$$190 \quad I_{\text{sat}}^t = \begin{cases} \frac{E_{\text{sat}}^t}{P_{\text{sat}}^t} (P^t - P_{\text{sat,max}}^t), & \text{if } P^t > P_{\text{sat,max}}^t \\ 0, & \text{otherwise} \end{cases} \quad (4)$$

$$I_{\text{dry}}^t = \begin{cases} S_{\text{canopy,max}}, & \text{if } P^t > P_{\text{sat,max}}^t \\ 0, & \text{otherwise} \end{cases} \quad (5)$$

The total interception I_{total}^t [mm] at time step t , assuming that trunk interception can be neglected, is the sum of the interception in all three phases, bounded by potential evapotranspiration $E_{\text{pot,total}}^t$:

$$I_{\text{total}}^t = \min(I_{\text{wet}}^t + I_{\text{dry}}^t + I_{\text{sat}}^t, E_{\text{pot,total}}^t). \quad (6)$$

195 Throughfall $P_{\text{throughfall}}^t$ [mm] at time step t is the remainder after subtracting the total interception and stemflow from the precipitation:

$$P_{\text{throughfall}}^t = P^t - I_{\text{total}}^t - P_{\text{stemflow}}^t. \quad (7)$$

The remaining potential evaporation $E_{\text{pot,remainder}}^t$ [mm] at time step t is given by:

$$E_{\text{pot,remainder}}^t = E_{\text{pot,total}}^t - I_{\text{total}}^t. \quad (8)$$

200 2.2.2 Modified Rutter model

For sub-daily time steps a modified Rutter interception model is used, which compared to the Gash model keeps track of the canopy storage S_{canopy}^t [mm] and is updated in two steps. Stemflow is calculated in the same way as the Gash model, see Eq. (2). The amount of precipitation P_{canopy}^t at time step t that falls on the canopy is a function of the total precipitation amount and the canopy gap and stemflow fractions:

$$205 \quad P_{\text{canopy}}^t = \max((1 - f_{\text{canopygap}} - f_{\text{stemflow}}), 0)P^t. \quad (9)$$

The initial drainage $D_{\text{canopy,s1}}^t$ [mm] from the canopy storage at time step t is the surplus of canopy storage at the previous time step compared to the canopy storage capacity $S_{\text{canopy,max}}$ [mm]:

$$D_{\text{canopy,s1}}^t = \begin{cases} (S_{\text{canopy}}^{t-1} - S_{\text{canopy,max}}), & \text{if } S_{\text{canopy}}^{t-1} > S_{\text{canopy,max}} \\ 0, & \text{otherwise.} \end{cases} \quad (10)$$



The canopy storage is then updated based on the initial canopy drainage, precipitation that falls on the canopy and the evapo-
 210 ration from the canopy storage ($\min(S_{\text{canopy}}^t, E_{\text{pot,total}}^t)$) [mm]:

$$S_{\text{canopy}}^t = S_{\text{canopy}}^{t-1} + P_{\text{canopy}}^t - D_{\text{canopy,s1}}^t, \quad (11)$$

$$S_{\text{canopy}}^t = S_{\text{canopy}}^t - \min(S_{\text{canopy}}^t, E_{\text{pot,total}}^t). \quad (12)$$

The remaining potential evaporation $E_{\text{pot,remainder}}^t$ [mm] at time step t is given by:

$$E_{\text{pot,remainder}}^t = E_{\text{pot,total}}^t - \min(S_{\text{canopy}}^t, E_{\text{pot,total}}^t). \quad (13)$$

215 The canopy storage S_{canopy}^t is drained again if required with drainage $D_{\text{canopy,s2}}^t$ at time step t :

$$D_{\text{canopy,s2}}^t = \begin{cases} (S_{\text{canopy}}^t - S_{\text{canopy,max}}), & \text{if } S_{\text{canopy}}^t > S_{\text{canopy,max}} \\ 0, & \text{otherwise} \end{cases} \quad (14)$$

and subtracted from S_{canopy}^t , to get the final canopy storage S_{canopy}^t [mm]:

$$S_{\text{canopy}}^t = S_{\text{canopy}}^t - D_{\text{canopy,s2}}^t. \quad (15)$$

Throughfall $P_{\text{throughfall}}^t$ [mm] at time step t is calculated as the total drainage from the canopy and the amount of precipitation
 220 that falls directly on the ground:

$$P_{\text{throughfall}}^t = D_{\text{canopy,s1}}^t + D_{\text{canopy,s2}}^t + f_{\text{canopygap}} P^t. \quad (16)$$

The total interception I_{total}^t [mm] at time step t is given by:

$$I_{\text{total}}^t = P^t - P_{\text{stemflow}}^t - P_{\text{throughfall}}^t \quad (17)$$

2.2.3 Interception model parameters from Leaf Area Index (LAI)

225 Within wflow_sbm it is possible to estimate interception model parameters based on monthly LAI maps (climatology). It is assumed that the canopy capacity for leaves $S_{\text{leaf,max}}^t$ is linearly related to LAI through the specific leaf storage S_{leaf} [mm] (Van Dijk and Bruijnzeel, 2001):

$$S_{\text{leaf,max}}^t = S_{\text{leaf}} \text{LAI}^t. \quad (18)$$



The specific leaf storage is related to land cover type. Also the storage for the woody part of the vegetation $S_{\text{wood,max}}$ is required to estimate total canopy capacity $S_{\text{canopy,max}}$ [mm]. The relations between land cover and S_{leaf} and $S_{\text{wood,max}}$ are based on Pitman (1989) and Liu (1998). The canopy gap fraction $f_{\text{canopygap}}^t$ [-] at time step t is determined by using the extinction coefficient k based on Van Dijk and Bruijnzeel (2001) and is related to land cover type:

$$f_{\text{canopygap}}^t = e^{(-kLAI^t)}. \quad (19)$$

2.3 Snow and glaciers

2.3.1 Snow

Snow processes are adopted from the HBV-96 hydrologic model concept (Bergström, 1992). Effective precipitation $P_{\text{effective}}^t$ [mm] (throughfall and stemflow) occurs as snowfall P_{snow}^t [mm] at time step t , if the air temperature T_{air}^t [°C] at time step t is below a user-defined temperature threshold $s_{\text{fall,Tthreshold}}$ [°C]. An interval parameter $s_{\text{fall,Tinterval}}$ [°C] defines the range over which precipitation is partly falling as snow, and partly as rain, with 100% snow at the lower end and decreasing linearly to 0% at the upper end. The fraction of precipitation that occurs as rainfall f_{rain}^t [-] at time step t is calculated as:

$$f_{\text{rain}}^t = \begin{cases} 0, & \text{if } s_{\text{fall,Tinterval}} = 0 \text{ \& } T_{\text{air}}^t \leq s_{\text{fall,Tthreshold}} \\ 1, & \text{if } s_{\text{fall,Tinterval}} = 0 \text{ \& } T_{\text{air}}^t > s_{\text{fall,Tthreshold}} \\ \max\left(\min\left(\frac{T_{\text{air}}^t - s_{\text{fall,Tthreshold}} - 0.5 s_{\text{fall,Tinterval}}}{s_{\text{fall,Tinterval}}}, 1\right), 0\right), & \text{if } s_{\text{fall,Tinterval}} \neq 0. \end{cases} \quad (20)$$

This fraction is used to calculate the snowfall amount P_{snow}^t and rainfall amount P_{rain}^t [mm] at time step t as follows:

$$P_{\text{snow}}^t = (1 - f_{\text{rain}}^t)P_{\text{effective}}^t, \quad (21)$$

$$P_{\text{rain}}^t = f_{\text{rain}}^t P_{\text{effective}}^t. \quad (22)$$

For snowmelt HBV-96 uses a degree-day approach, an empirical relationship between melt and air temperature. If T_{air}^t is above a melting temperature threshold $s_{\text{melt,Tthreshold}}$ [°C], snowmelt occurs. The potential snowmelt $M_{\text{snow,pot}}^t$ at time step t , using the degree-day factor s_{ddf} [mm t^{-1} °C $^{-1}$], is calculated as follows:

$$M_{\text{snow,pot}}^t = \begin{cases} s_{\text{ddf}}(T_{\text{air}}^t - s_{\text{melt,Tthreshold}}), & \text{if } T_{\text{air}}^t > s_{\text{melt,Tthreshold}} \\ 0, & \text{otherwise.} \end{cases} \quad (23)$$

The actual snowmelt $M_{\text{snow,act}}^t$ [mm] at time step t is limited by the snow storage S_{snow}^{t-1} [mm] at the end of the previous time step, and is calculated by taking the minimum of $M_{\text{snow,pot}}^t$ and S_{snow}^{t-1} . The snow pack retains water that can refreeze if T_{air}^t is



below $s_{\text{melt},T_{\text{threshold}}}$. The potential amount of water that can refreeze $M_{\text{refreeze,pot}}^t$ [mm] at time step t , is controlled by s_{ddf} , a coefficient of refreezing s_{refreeze} [-] (fixed: 0.05), T_{air}^t and $s_{\text{melt},T_{\text{threshold}}}$ as follows:

$$M_{\text{refreeze,pot}}^t = \begin{cases} s_{\text{ddf}} s_{\text{refreeze}} (s_{\text{melt},T_{\text{threshold}}} - T_{\text{air}}^t), & \text{if } T_{\text{air}}^t < s_{\text{melt},T_{\text{threshold}}} \\ 0, & \text{otherwise.} \end{cases} \quad (24)$$

255 The actual amount that can refreeze, $M_{\text{refreeze,act}}^t$ [mm] is based on the amount of snow water $S_{\text{snow,liquid}}^{t-1}$ at the previous time step and the potential amount of water that can refreeze $M_{\text{refreeze,pot}}^t$, by taking the minimum of $M_{\text{refreeze,pot}}^t$ and $S_{\text{snow,liquid}}^{t-1}$. Snow pack storage S_{snow}^t [mm] at time step t is then a function of snow pack storage at the previous time step (S_{snow}^{t-1}), snowfall amount, actual refreezing amount and actual snowmelt at time step t :

$$S_{\text{snow}}^t = S_{\text{snow}}^{t-1} + P_{\text{snow}}^t + M_{\text{refreeze,act}}^t - M_{\text{snow,act}}^t. \quad (25)$$

260 The liquid water content of snow $S_{\text{snow,liquid}}^t$ [mm] at time step t is a function of the liquid water content of snow at the previous time step ($S_{\text{snow,liquid}}^{t-1}$ [mm]), actual refreezing amount, actual snowmelt and rainfall amount at time step t , and the maximum amount of water that the snowpack can hold. This maximum amount is controlled by the water holding capacity s_{whc} [-] of snow and the snow pack storage at time step t :

$$S_{\text{snow,liquid}}^t = S_{\text{snow,liquid}}^{t-1} - M_{\text{refreeze,act}}^t + M_{\text{snow,act}}^t + P_{\text{rain}}^t, \quad (26)$$

$$S_{\text{snow,liquid}}^t = S_{\text{snow,liquid}}^t - \max(S_{\text{snow,liquid}}^t - S_{\text{snow}}^t s_{\text{whc}}, 0). \quad (27)$$

265 The amount that does exceed the fraction of the current snow pack ($\max(S_{\text{snow,liquid}}^t - S_{\text{snow}}^t s_{\text{whc}}, 0)$) is available as rainfall at time step t .

To control unlimited build-up of the snow pack at high altitude where temperature rarely reaches above melting temperature, the optional avalanche routine can be used to transport snow downhill based on the local drain network, where it becomes available for snow melt. The fraction of snow that can be transported downhill is calculated as:

$$270 \quad f_{\text{snow transport}}^t = \min(0.5, \frac{c_{\text{land slope}}}{\tan(80^\circ)}) \min(1, \frac{S_{\text{snow}}^t}{s_{\text{max}}}), \quad (28)$$

with $f_{\text{snow transport}}^t$ [-] the fraction of snow at time step t that is available for transport downhill, $c_{\text{land slope}}$ [m m^{-1}] the slope of the land surface and s_{max} [mm] the maximum snow pack with a fixed value of 10,000 mm. The fraction of snow that can be transported downhill is multiplied with the snow pack storage, and gives the transport capacity of snow $M_{\text{snow,downhill}}^t$ [mm] at time step t :



$$275 \quad M_{\text{snow,downhill}}^t = S_{\text{snow}}^t f_{\text{snow transport}}^t \quad (29)$$

Snow is then transported downhill, based on the local drain network and the transport capacity of snow that limits the snow transport, updating the amount of snow S_{snow}^t [mm] and liquid water content of snow $S_{\text{snow,liquid}}^t$ [mm] in each grid cell at time step t .

2.3.2 Glaciers

280 Glacier modelling considers two main processes: glacier build-up from snow turning into firn/ice (adopted from the HBV-light model; Seibert et al., 2018) and glacier melt (using a temperature degree-day model). First, a fixed fraction $g_{\text{snow to ice}}$, that typically ranges between 0.001 and 0.006, of the snowpack S_{snow}^t [mm] on top of the glacier is converted into ice for each time step:

$$S_{\text{snow to ice}}^t = \min(g_{\text{snow to ice}} S_{\text{snow}}^t, 8 \frac{t}{t_b}), \quad (30)$$

285 where $S_{\text{snow to ice}}^t$ [mm] is the amount of snow converted into ice at time step t , with a maximum conversion rate of 8 mm day⁻¹. This maximum conversion rate is scaled by the the model time step t [s], and the model base time step t_b of 86,400 [s]. The snow pack from the snow module (section 2.3.1) S_{snow}^t [mm] at time step t is then updated as follows:

$$S_{\text{snow}}^t = S_{\text{snow}}^t - (S_{\text{snow to ice}}^t f_{\text{glacier}}), \quad (31)$$

with f_{glacier} [-] the fraction of a grid cell covered by a glacier. When the snowpack on top of the glacier is almost all melted
 290 ($S_{\text{snow}}^t < 10$ mm), glacier melt is enabled and estimated with a degree-day model. If the air temperature T_{air}^t is above a melting temperature threshold $g_{\text{melt,Tthreshold}}$ [°C], glacier melt occurs. The potential glacier melt $M_{\text{glacier,pot}}^t$ [mm], using the degree-day factor g_{ddf} [mm t⁻¹ °C⁻¹], is calculated as:

$$M_{\text{glacier,pot}}^t = \begin{cases} g_{\text{ddf}}(T_{\text{air}}^t - g_{\text{melt,Tthreshold}}), & \text{if } T_{\text{air}}^t > g_{\text{melt,Tthreshold}} \\ 0, & \text{otherwise.} \end{cases} \quad (32)$$

The actual glacier melt $M_{\text{glacier,act}}^t$ [mm] at time step t is limited by the sum of the glacier storage at the end of the previous
 295 time step S_{glacier}^{t-1} [mm] (expressed in mm water equivalent) and $S_{\text{snow to ice}}^t$:

$$M_{\text{glacier,act}}^t = \min(M_{\text{glacier,pot}}^t, S_{\text{glacier}}^{t-1} + S_{\text{snow to ice}}^t). \quad (33)$$

The glacier storage S_{glacier}^t [mm] at time step t is then updated as follows:



$$S_{\text{glacier}}^t = S_{\text{glacier}}^{t-1} + S_{\text{snow to ice}}^t - M_{\text{glacier,act}}^t \quad (34)$$

A map with S_{glacier} values can be provided as an initial state (default: 5500 mm) when wflow_sbm is initialized with default values in the code (“cold” start), see also Table A2.

2.4 The soil module and evapotranspiration

2.4.1 Infiltration

Water available for infiltration $F_{\text{available}}^t$ [mm] at time step t into the soil (throughfall, stemflow, snow and glacier melt) is first added to the saturated parts of the grid cell: the river flow and overland flow components of wflow_sbm. This is based on the river fraction f_{river} [-] (river flow component) and open water fraction (excluding rivers) $f_{\text{open water}}$ [-] (overland flow component) within a grid cell, as follows:

$$R_{\text{river}}^t = f_{\text{river}} F_{\text{available}}^t \quad (35)$$

$$R_{\text{open water}}^t = f_{\text{open water}} F_{\text{available}}^t \quad (36)$$

where R_{river}^t [mm] is runoff from the river fraction in a cell at time step t , and $R_{\text{open water}}^t$ [mm] is runoff from the open water fraction in a cell at time step t . R_{river}^t and $R_{\text{open water}}^t$ are later added to the wflow_sbm river and overland flow components respectively. The remaining water available for infiltration $F_{\text{available}}^t$ at time step t into the soil is determined as:

$$F_{\text{available}}^t = F_{\text{available}}^t - R_{\text{river}}^t - R_{\text{open water}}^t \quad (37)$$

The soil in wflow_sbm is considered as a bucket with a depth z_{soil} [mm], and is divided into a saturated store S_{sat} [mm] and an unsaturated store S_{unsat} [mm]. The top of the saturated store forms a pseudo-water table at depth $z_{\text{watertable}}$ [mm] such that the value of S_{sat} is given by:

$$S_{\text{sat}} = (z_{\text{soil}} - z_{\text{watertable}})(\theta_s - \theta_r), \quad (38)$$

where θ_s and θ_r are the saturated and residual soil water contents, respectively, both expressed as mm mm^{-1} . The amount of water that can infiltrate is a function of the infiltration capacity $c_{\text{infiltration,paved}}$ [mm day^{-1}] of the compacted soil (or paved area) fraction (f_{paved} [-]) of each grid cell, the infiltration capacity $c_{\text{infiltration,unpaved}}$ [mm day^{-1}] of the non-compacted soil fraction (or unpaved area) ($(1 - f_{\text{paved}})$) of each gridcell, the storage capacity of the unsaturated zone S_{unsat}^{t-1} [mm] at the previous time step, and an optional reduction factor f_{frozen} applied to the infiltration capacity when snow is modelled. The



parameter f_{frozen} depends on the near-surface soil temperature which is modelled based on the approach of Wigmosta et al. (2009):

$$T_{\text{soil}}^t = T_{\text{soil}}^{t-1} + w(T_{\text{air}}^t - T_{\text{soil}}^{t-1}), \quad (39)$$

325 where T_{soil}^t [$^{\circ}\text{C}$] is the near-surface soil temperature at time step t , T_{air}^t [$^{\circ}\text{C}$] is the air temperature at time step t , T_{soil}^{t-1} [$^{\circ}\text{C}$] is the near-surface soil temperature at the previous time step, and w is a weighting coefficient [-]. The optional infiltration capacity reduction factor f_{frozen}^t at time step t is based on the model parameter $f_{\text{red,frozen}}$ [-] and the near-surface soil temperature as follows:

$$f_{\text{frozen}}^t = \begin{cases} \frac{1.0}{b + e^{(-c(T_{\text{soil}}^t - a))}} + f_{\text{red,frozen}}, & \text{if snow \& soilinfreduction} \\ 1, & \text{otherwise,} \end{cases} \quad (40)$$

330 where $b = \frac{1.0}{(1.0 - f_{\text{red,frozen}})}$, $a = 0.0$ and $c = 8.0$. The initial storage capacity of the unsaturated zone $S_{\text{unsat,max}}^t$ [mm] at time step t is based on the saturated storage S_{sat}^{t-1} [mm] at the previous time step, the sum of unsaturated storage for n unsaturated soil layers ($\sum S_{\text{unsat,n}}^{t-1}$ [mm] at the previous time step), and the total soil water capacity of the wflow_sbm soil bucket. $S_{\text{unsat,max}}^t$ is calculated as follows:

$$S_{\text{unsat,max}}^t = z_{\text{soil}}(\theta_s - \theta_r) - S_{\text{sat}}^{t-1} - \sum S_{\text{unsat,n}}^{t-1}. \quad (41)$$

335 The total available water for infiltration is split into two parts, the part that falls on compacted areas $F_{\text{available}}^t f_{\text{paved}}$ [mm] and the part that falls on non-compacted areas $F_{\text{available}}^t (1 - f_{\text{paved}})$ [mm] at time step t . The maximum amount of water that can infiltrate in these areas is calculated by taking the minimum of the infiltration capacity and the available water for infiltration in these areas:

$$F_{\text{unpaved}}^t = \min(c_{\text{infiltration,unpaved}} f_{\text{frozen}}^t, F_{\text{available}}^t (1 - f_{\text{paved}})), \quad (42)$$

340

$$F_{\text{paved}}^t = \min(c_{\text{infiltration,paved}} f_{\text{frozen}}^t, F_{\text{available}}^t f_{\text{paved}}). \quad (43)$$

The water that can actually infiltrate F_{total}^t [mm] is calculated by taking the minimum of the total water that can infiltrate (compacted and non-compacted areas) and the initial unsaturated storage capacity:

$$F_{\text{total}}^t = \min(F_{\text{unpaved}}^t + F_{\text{paved}}^t, S_{\text{unsat,max}}^t). \quad (44)$$

345 Finally, the amount of infiltration excess water F_{excess}^t [mm] at time step t is determined as:

$$F_{\text{excess}}^t = (F_{\text{available}}^t (1 - f_{\text{paved}}) - F_{\text{unpaved}}^t) + (F_{\text{available}}^t f_{\text{paved}} - F_{\text{paved}}^t). \quad (45)$$



2.4.2 Soil water accounting scheme

The bucket in wflow_sbm with a depth z_{soil} can be split-up in different layers. Assuming a unit head gradient, the transfer of water $Q_{\text{transfer},n}$ [mm t^{-1}] from an unsaturated store layer is controlled by the vertical saturated hydraulic conductivity K_{vz} at depth z of the bottom layer (transfer between unsaturated store layers) or the pseudo-water table at depth $z_{\text{watertable}}$ (transfer to the saturated store), the effective saturation degree of the layer, and a Brooks-Corey power coefficient (c_n) based on the pore size distribution index λ (Brooks and Corey, 1964):

$$Q_{\text{transfer},n} = K_{vz} \left(\frac{\theta - \theta_r}{\theta_s - \theta_r} \right)^{c_n}, \quad (46)$$

$$c_n = \frac{2 + 3\lambda}{\lambda}. \quad (47)$$

Vertical saturated hydraulic conductivity K_{vz} [mm t^{-1}] declines with soil depth z in wflow_sbm according to:

$$K_{vz} = K_{v0} e^{(-f_{Kv}z)} \quad (48)$$

where the model parameter K_{v0} [mm t^{-1}] is the vertical saturated conductivity at the soil surface and f_{Kv} is a scaling parameter [mm^{-1}]. For n unsaturated soil layers ($> z_{\text{watertable}}^{t-1}$), the transfer of water is calculated as follows:

$$S_{\text{unsat},n}^t = S_{\text{unsat},n}^{t-1} + Q_{\text{in},n}^t, \quad (49)$$

$$Q_{\text{transfer},n}^t = f_{Kv,n} (K_{v0}) e^{(-f_{Kv}z_n)} \min \left(\left(\frac{S_{\text{unsat},n}^t}{z_{n,\text{thickness}}(\theta_s - \theta_r)} \right)^{c_n}, 1 \right), \quad (50)$$

$$S_{\text{unsat},n}^t = S_{\text{unsat},n}^{t-1} - \min(Q_{\text{transfer},n}^t, S_{\text{unsat},n}^{t-1}), \quad (51)$$

where $Q_{\text{in},n}^t$ for unsaturated soil layer $n = 1$ (upper soil layer) is F_{total}^t , and for unsaturated soil layer $n > 1$, $Q_{\text{in},n}^t$ is $\min(Q_{\text{transfer},n-1}^t, S_{\text{unsat},n-1}^t, S_{\text{unsat},n}^{t-1})$ [mm] the unsaturated storage of layer n at the previous time step, $S_{\text{unsat},n}^t$ [mm] the subsequent updated unsaturated storage of layer n at time step t , $f_{Kv,n}$ is a multiplication factor [-] for each soil layer n , and $z_{n,\text{thickness}}$ [mm] the soil layer thickness of soil layer n .

When the bucket in wflow_sbm is not split-up into different layers, it is possible to use the original Topog_SBM vertical transfer formulation. The transfer of water from the unsaturated store to the saturated store is in that case controlled by the vertical saturated hydraulic conductivity K_{vz} at depth $z_{\text{watertable}}^{t-1}$ and the ratio between the unsaturated store and the saturation deficit S_{deficit}^t at time step t :



$$370 \quad S_{\text{deficit}}^t = (\theta_s - \theta_r)z_{\text{soil}} - S_{\text{sat}}^{t-1}, \quad (52)$$

$$Q_{\text{transfer},n}^t = f_{Kv,1}(K_{v0})e^{(-f_{Kv}z_{\text{watertable}}^{t-1})} \frac{S_{\text{unsat},1}^t}{S_{\text{deficit}}^t}. \quad (53)$$

2.4.3 Evapotranspiration

Open water evaporation from water bodies (excluding rivers) $E_{\text{open water}}^t$ and rivers E_{river}^t at time step t is based on: the fraction of open water $f_{\text{open water}}$ [-], the fraction of rivers f_{river} [-], the water level in the kinematic reservoir of the river flow component $S_{\text{wl,river}}^{t-1}$ [mm] and the overland flow component $S_{\text{wl,land}}^{t-1}$ at the previous time step, and the remaining potential evaporation after interception $E_{\text{pot,remainder}}^t$ [mm] as follows:

$$E_{\text{river}}^t = \min(S_{\text{wl,river}}^{t-1}f_{\text{river}}, f_{\text{river}}E_{\text{pot,remainder}}^t), \quad (54)$$

$$E_{\text{open water}}^t = \min(S_{\text{wl,land}}^{t-1}f_{\text{open water}}, f_{\text{open water}}E_{\text{pot,remainder}}^t). \quad (55)$$

The potential evaporation remaining after interception (Eq. (8) or (13)) and open water evaporation (rivers and water bodies (excluding rivers)) $E_{\text{pot,remainder}}^t$ [mm] at time step t is then:

$$E_{\text{pot,remainder}}^t = E_{\text{pot,remainder}}^t - E_{\text{river}}^t - E_{\text{open water}}^t. \quad (56)$$

Potential soil evaporation $E_{\text{pot,soil}}^t$ [mm] at time step t is based on $E_{\text{pot,remainder}}^t$ and the canopy gap fraction $f_{\text{canopygap}}^t$ [-] (assumed to be identical to the amount of bare soil). When the bucket in wflow_sbm is not split-up into different layers, soil evaporation $E_{\text{act,soil}}^t$ [mm] is calculated as follows:

$$385 \quad E_{\text{pot,soil}}^t = E_{\text{pot,remainder}}^t f_{\text{canopygap}}^t, \quad (57)$$

$$E_{\text{act,soil}}^t = \min(E_{\text{pot,soil}}^t \frac{S_{\text{deficit}}^t}{z_{\text{soil}}(\theta_s - \theta_r)}, S_{\text{unsat},1}^t). \quad (58)$$

As such, soil evaporation will be potential if the soil is fully wetted and it decreases linearly with increasing soil moisture deficit. When the bucket in wflow_sbm is split-up into different layers, soil evaporation $E_{\text{act,soil}}^t$ [mm] is restricted to the upper layer. As for the case of one single soil layer, potential soil evaporation is scaled according to the wetness of the soil layer, based on the unsaturated layer storage from Eq. (51), as follows:

$$E_{\text{act,soil}}^t = \begin{cases} \min(E_{\text{pot,soil}}^t \frac{S_{\text{unsat},1}^t}{z_{\text{watertable}}^{t-1}(\theta_s - \theta_r)}, S_{\text{unsat},1}^t), & \text{if } z_{\text{watertable}}^{t-1} \leq z_{1,\text{thickness}} \\ \min(E_{\text{pot,soil}}^t \frac{S_{\text{unsat},1}^t}{z_{1,\text{thickness}}(\theta_s - \theta_r)}, S_{\text{unsat},1}^t), & \text{if } z_{\text{watertable}}^{t-1} > z_{1,\text{thickness}} \end{cases} \quad (59)$$



Soil evaporation $E_{act,soil}^t$ is subtracted from the upper soil layer $S_{unsat,1}^t$ (Eq. 51), and the remaining potential soil evaporation $E_{remainder,soil}^t$ is determined as follows:

$$S_{unsat,1}^t = S_{unsat,1}^t - E_{act,soil}^t, \quad (60)$$

$$395 \quad E_{remainder,soil}^t = E_{pot,soil}^t - E_{act,soil}^t. \quad (61)$$

When the bucket in `wflow_sbm` is split-up into different layers, soil evaporation $E_{act,soil,sat}^t$ [mm] from the saturated store is possible, when the water table $z_{watertable}^{t-1}$ is present in the upper soil layer, and calculated as follows:

$$E_{act,soil,sat}^t = \min(E_{remainder,soil}^t \frac{z_{1,thickness} - z_{watertable}^{t-1}}{z_{1,thickness}}, (z_{1,thickness} - z_{watertable}^{t-1})(\theta_s - \theta_r)), \quad (62)$$

and subtracted from the saturated store (at the previous time step):

$$400 \quad S_{sat}^t = S_{sat}^{t-1} - E_{act,soil,sat}^t. \quad (63)$$

Potential evaporation $E_{pot,remainder}^t$ [mm] that is available for transpiration, is based on the remaining potential evaporation after interception and open water evaporation (Eq. 56) and the canopy gap fraction, as follows:

$$E_{pot,remainder}^t = E_{pot,remainder}^t (1.0 - f_{canopygap}^t). \quad (64)$$

In `wflow_sbm`, transpiration is first taken from the saturated store if the roots reach the water table $z_{watertable}^{t-1}$ at the previous
 405 time step. The fraction of wet roots $f_{wet\ roots}$ [-] (ranging between 0 and 1) is determined using a sigmoid function, that defines the sharpness of the transition between fully wet and fully dry roots. Transpiration $E_{trans,sat}^t$ from the saturated store at time step t is calculated as follows:

$$f_{wet\ roots} = \frac{1.0}{1.0 + e^{(-c_{rd}(z_{watertable}^{t-1} - z_{rooting}))}}, \quad (65)$$

$$E_{trans,sat}^t = \begin{cases} \min(E_{pot,remainder}^t f_{wet\ roots}, S_{sat}^t), & \text{multiple soil layers} \\ \min(E_{pot,remainder}^t f_{wet\ roots}, S_{sat}^{t-1}), & \text{otherwise,} \end{cases} \quad (66)$$

410 where c_{rd} is a model parameter that controls the sharpness of the sigmoid function and $z_{rooting}$ [mm] is the rooting depth. The saturated store is then updated as follows (in case of multiple soil layers S_{sat}^t is given by Eq. (63)):



$$S_{\text{sat}}^t = \begin{cases} S_{\text{sat}}^t - E_{\text{trans,sat}}^t, & \text{multiple soil layers} \\ S_{\text{sat}}^{t-1} - E_{\text{trans,sat}}^t, & \text{otherwise.} \end{cases} \quad (67)$$

The remaining potential evaporation $E_{\text{pot,remainder}}^t$ [mm] available for transpiration from the unsaturated store is updated $E_{\text{trans,sat}}^t$ as follows:

$$415 \quad E_{\text{pot,remainder}}^t = E_{\text{pot,remainder}}^t - E_{\text{trans,sat}}^t. \quad (68)$$

The maximum allowed water extraction by roots $E_{\text{root,max,n}}^t$ at time step t is a function of the fraction of roots $f_{\text{roots,n}}^t$ [-] per unsaturated layer n , and the available unsaturated store layer depth [mm] of layer n :

$$E_{\text{root,max,n}}^t = f_{\text{roots,n}}^t S_{\text{unsat}}^t. \quad (69)$$

Next, a root water uptake reduction model based on Feddes et al. (1978) is used to calculate a reduction coefficient as a function
 420 of soil matric suction. Soil matric suction is calculated following Brooks and Corey (1964):

$$\frac{(\theta - \theta_r)}{(\theta_s - \theta_r)} = \begin{cases} \left(\frac{h_b}{h}\right)^\lambda, & h > h_b \\ 1, & h \leq h_b, \end{cases} \quad (70)$$

where h is the soil matric suction [cm], h_b is the air entry value [cm], and θ , θ_r , θ_s and λ as previously defined. In wflow_sbm soil matric suction h_n^t for each unsaturated soil layer n at time step t is calculated as follows:

$$h_n^t = \frac{h_b}{\left(\frac{S_{\text{unsat,n}}^t / z_{\text{n,thickness}}^t}{(\theta_s - \theta_r)}\right)^{\lambda_n^{-1}}}, \quad (71)$$

425 where $S_{\text{unsat,1}}^t$ is given by Eq. (60), and for unsaturated layers $n > 1$ $S_{\text{unsat,n}}^t$ is given by Eq. (51). The root water uptake reduction coefficient $f_{\text{root uptake,n}}^t$ at time step t with h_n^t below or equal h_3 (400 cm) is set to 1, with h_n^t above or equal to h_4 (15849 cm) $f_{\text{root uptake,n}}^t$ is 0, and with h_n^t between h_3 and h_4 $f_{\text{root uptake,n}}^t$ declines linearly from 1 to 0. The values for h_2 (100 cm), h_3 and h_4 are fixed, and h_1 (default: 10 cm) can be defined as input to the model. In the original transpiration reduction-curve of Feddes et al. (1978) root water uptake above h_1 is set to zero (oxygen deficit) and between h_1 and h_2 root
 430 water uptake is limited. The assumption that very wet conditions do not affect root water uptake too much is probably generally applicable to natural vegetation, however for crops this assumption is not valid. This could be improved in the Wflow.jl code by applying the reduction to crops only. While the h_3 value is fixed, in the original transpiration reduction-curve of Feddes et al. (1978) h_3 varies with the potential transpiration rate, and this could also be improved in the code. For unsaturated soil layer



435 n transpiration $E_{\text{trans,unsat},n}^t$ [mm] is controlled by $E_{\text{root,max},n}^t$, the remaining evaporation $E_{\text{pot,remainder}}^t$ [mm] (Eq. 68), the
 unsaturated storage $S_{\text{unsat},n}^t$ [mm] (for soil layer $n = 1$ see Eq. (60) and for layers $n > 1$ see Eq. (51)), and $f_{\text{root uptake},n}^t$, at
 time step t :

$$E_{\text{trans,unsat},n}^t = \min(E_{\text{root,max},n}^t, E_{\text{pot,remainder}}^t, S_{\text{unsat},n}^t) f_{\text{root uptake},n}^t \quad (72)$$

At the same time $S_{\text{unsat},n}^t$ and the remaining potential evaporation $E_{\text{pot,remainder}}^t$ [mm] are updated by subtracting $E_{\text{trans,unsat},n}^t$:

$$S_{\text{unsat},n}^t = S_{\text{unsat},n}^t - E_{\text{trans,unsat},n}^t \quad (73)$$

$$440 \quad E_{\text{pot,remainder}}^t = E_{\text{pot,remainder}}^t - E_{\text{trans,unsat},n}^t \quad (74)$$

After the soil water transfer, evaporation and transpiration computations, a soil water balance check is performed. Unsaturated storage that exceeds the maximum storage per layer, is transferred to the layer above (or surface), from the bottom to the top unsaturated soil layer, resulting in excess water at the surface $R_{\text{excess,unsat}}^t$ [mm]. The water that actually infiltrates F_{act}^t [mm] is then calculated as follows:

$$445 \quad F_{\text{act}}^t = F_{\text{total}}^t - R_{\text{excess,unsat}}^t \quad (75)$$

and the amount of water that cannot infiltrate due to saturated soil conditions $F_{\text{excess,sat}}^t$ [mm] is determined as:

$$F_{\text{excess,sat}}^t = F_{\text{available}}^t - F_{\text{total}}^t - F_{\text{excess}}^t + R_{\text{excess,unsat}}^t \quad (76)$$

Capillary rise in `wflow_sbm` is determined using the following approach, first $K_{\text{vz watertable}}^t$ at time step t is determined based on the water table $z_{\text{watertable}}^{t-1}$ at the previous time step:

$$450 \quad K_{\text{vz watertable}}^t = f_{Kv,n}(K_{v0})e^{-f_{Kv}z_{\text{watertable}}^{t-1}}, \quad (77)$$

where $f_{Kv,n}$ is the multiplication factor for soil layer n where $z_{\text{watertable}}^{t-1}$ is present. Then a maximum capillary rise is determined from the minimum of $K_{\text{vz watertable}}^t$, the actual transpiration taken from the unsaturated store $\sum E_{\text{trans,unsat},n}^t$, S_{sat}^t (Eq. 67), and the unsaturated store capacity $S_{\text{unsat,max}}^t$ which is based on S_{sat}^t (Eq. 67) and $\sum S_{\text{unsat},n}^t$ (soil water balance check after Eq. (73)):

$$455 \quad S_{\text{unsat,max}}^t = z_{\text{soil}}(\theta_s - \theta_r) - S_{\text{sat}}^t - \sum S_{\text{unsat},n}^t \quad (78)$$

$$C_{\text{max}}^t = \max(0.0, \min(K_{\text{vz watertable}}^t, \sum E_{\text{trans,unsat},n}^t, S_{\text{unsat,max}}^t, S_{\text{sat}}^t)). \quad (79)$$



Finally the maximum capillary rise is scaled using the following empirical equation (e.g., Zammouri, 2001; Yang et al., 2011; Wang et al., 2016):

$$C_{\text{act}}^t = \begin{cases} C_{\text{max}}^t \left(1 - \frac{z_{\text{watertable}}^{t-1}}{z_{\text{cap,maxdepth}}}\right)^m, & \text{if } z_{\text{watertable}}^{t-1} < z_{\text{cap,maxdepth}} \\ 0, & \text{otherwise,} \end{cases} \quad (80)$$

460 where C_{act}^t [mm] is the capillary rise at time step t , $z_{\text{cap,maxdepth}}$ [mm] is the critical water depth beyond which capillary rise ceases and m [-] is an empirical coefficient related to soil properties and climate, generally set between 1-3. When the bucket in `wflow_sbm` is split-up into different layers, C_{act}^t is divided over the different unsaturated soil layers, from the bottom to the top unsaturated soil layer, without exceeding θ_s .

2.4.4 Leakage

465 In `wflow_sbm` it is possible to have leakage L^t at time step t from the saturated store S_{sat}^t (Eq. 67) to deeper groundwater, by setting the maximum leakage model parameter L_{max} [mm] > 0. This water is lost from the saturated store and runs out of the model domain. L^t is calculated as follows:

$$L^t = \min(K_{v0} e^{-f_{Kv} z_{\text{soil}}}, S_{\text{sat}}^t, L_{\text{max}}). \quad (81)$$

2.5 Lateral subsurface flow

470 In `wflow_sbm` the kinematic wave approach is used to route subsurface flow laterally. The saturated store can be drained laterally by saturated downslope subsurface flow for a slope with width w [m] according to:

$$Q_{\text{subsurface}} = \frac{K_{h0} c_{\text{land slope}}}{f_{Kv}} \left(e^{-f_{Kv} z_{\text{ssf,watertable}}} - e^{-f_{Kv} z_{\text{ssf,soil}}} \right) w, \quad (82)$$

where $c_{\text{land slope}}$ is the land slope [-], $Q_{\text{subsurface}}$ is subsurface flow [$\text{m}^3 \text{t}^{-1}$], $K_{h0} = 0.001 K_{v0} f_{Kh0} \frac{t_b}{t}$ is the horizontal saturated hydraulic conductivity at the soil surface [m day^{-1}], based on the vertical saturated conductivity at the soil surface K_{v0} [475 mm t^{-1}] and a multiplication factor f_{Kh0} [-], $z_{\text{ssf,watertable}}$ [m] is the water table depth (set by $z_{\text{watertable}}$ [mm] after unit conversion at the start of the lateral subsurface flow computation) and $z_{\text{ssf,soil}}$ [m] is the soil depth (set by z_{soil} [mm] after unit conversion). Combining with the following continuity equation:

$$(\theta_s - \theta_r) w \frac{\partial h}{\partial t} = - \frac{\partial Q_{\text{subsurface}}}{\partial x} + w R_{\text{input}} \quad (83)$$

where h is the water table height [m], x is the distance downslope [m], w is the flow width [m], and R_{input} is the netto input 480 rate [m t^{-1}] to the saturated store, substituting for $h(\frac{\partial q}{\partial h})$, gives:



$$\frac{\partial Q_{\text{subsurface}}}{\partial t} = -c \frac{\partial Q_{\text{subsurface}}}{\partial x} + cwR_{\text{input}}, \text{ with celerity } c = \frac{K_{h0} c_{\text{land slope}}}{(\theta_s - \theta_r)} e^{(-f_{Kv} z_{\text{ssf, watertable}})}. \quad (84)$$

The kinematic wave equation for lateral subsurface flow is solved iteratively using Newton's method. In wflow_sbm, the flow width w is calculated for each grid cell by dividing the cell area with the distance downslope x , based on the flow direction and the length in the x and y direction of each grid cell. The land slope $c_{\text{land slope}}$ needs to be provided for each grid cell in wflow_sbm. The netto input rate R_{input} in wflow_sbm consists of the input of transfer of soil water from the unsaturated soil layer above the water table $z_{\text{watertable}}^{t-1}$ [mm] at the previous time step, and the losses through capillary rise C_{act}^t , transpiration $E_{\text{act, soil, sat}}^t$ from the saturated store, leakage L^t and soil evaporation $E_{\text{act, soil}}^t$ from the saturated store, converted to m. After the lateral subsurface flow calculation, that is bounded by the maximum lateral subsurface flow rate based on $z_{\text{ssf, soil}}$, a check is made to determine if saturation of the entire soil column occurs, and as a consequence saturation excess overland flow is triggered. Water exfiltrating during saturated conditions $R_{\text{exfilt, sat}}^t$ [m] is calculated as follows:

$$R_{\text{exfilt, sat}}^t = \max\left(0, \frac{(Q_{\text{subsurface, in}}^t + R_{\text{input}}wx - Q_{\text{subsurface, out}}^t)}{wx} - z_{\text{ssf, watertable}}^t(\theta_s - \theta_r)\right), \quad (85)$$

where $Q_{\text{subsurface, in}}^t$ [$\text{m}^3 \text{ day}^{-1}$] is the subsurface flow in to a cell, $Q_{\text{subsurface, out}}^t$ [$\text{m}^3 \text{ day}^{-1}$] is the subsurface flow out of a cell, $z_{\text{ssf, watertable}}^t$ [m] is the water table depth, at time step t , and R_{input} , w , x , θ_s and θ_r as previously defined. Additionally, after the lateral subsurface flow calculation wflow_sbm checks if exfiltration $R_{\text{exfilt, unsat}}^t$ [mm] of the unsaturated store onto the land surface occurs because of a change in water table depth $z_{\text{watertable}}$ [mm] (set by $z_{\text{ssf, watertable}}^t$ after unit conversion). This check is performed from the bottom unsaturated layer (at the previous time step) until the top unsaturated layer, where the excess of unsaturated storage for each layer is transferred from the bottom to the top unsaturated layer, and can result in exfiltration of water onto the land surface.

2.6 Surface flow routing

The kinematic wave approach is used for river and overland flow routing. The kinematic wave equations are (Chow et al., 1988):

$$\frac{dQ}{dx} + \frac{dA}{dt} = Q_{\text{inflow}}, \quad (86)$$

$$A = \alpha Q^\beta, \quad (87)$$

and can be combined as follows:

$$\frac{dQ}{dx} + \alpha\beta Q^{\beta-1} \frac{dQ}{dt} = Q_{\text{inflow}}, \quad (88)$$



where Q is the surface runoff in the kinematic wave [$\text{m}^3 \text{s}^{-1}$], x is the length of the runoff pathway [m], A is the cross-section area of the runoff pathway [m^2], Q_{inflow} is the lateral inflow per unit length into the kinematic wave [$\text{m}^2 \text{s}^{-1}$], t is the integration time step [s] and α and β are coefficients. These coefficients can be determined by using Manning's equation (Chow et al., 1988), resulting in:

$$510 \quad \alpha = \left(\frac{nP^{\frac{2}{3}}}{\sqrt{c_{\text{slope}}}} \right)^{\beta} \quad \text{and} \quad \beta = 0.6, \quad (89)$$

where P [m] is the wetted perimeter, c_{slope} ($c_{\text{land slope}}$ for overland flow and $c_{\text{river slope}}$ for river flow) is the slope [m m^{-1}], and n (n_{land} for overland flow and n_{river} for river flow) is Manning's coefficient [$c_{\text{slope}} \text{m}^{-\frac{1}{3}}$]. The wetted perimeter P for river flow is calculated by adding the river width (w_{river}) and two times half of the river bankfull depth (h_{bankfull}). For overland flow, P is set equal to the effective flow width, determined by dividing the grid cell area by the flow length, and subtracting
 515 w_{river} . In wflow_sbm for river flow the parameters w_{river} , length (x_{river}) and $c_{\text{river slope}}$, and for overland flow $c_{\text{land slope}}$, need to be provided. The lateral inflow Q_{inflow} per unit flow length for overland flow routing consists of infiltration excess water F_{excess}^t , saturation excess water during infiltration $F_{\text{excess,sat}}^t$, exfiltration water from the unsaturated store $R_{\text{exfilt,unsat}}^t$, water exfiltrating during saturated conditions $R_{\text{exfilt,sat}}^t$, runoff from open water $R_{\text{open water}}^t$, and open water evaporation loss $E_{\text{open water}}^t$, converted to $\text{m}^2 \text{s}^{-1}$. The lateral inflow Q_{inflow} per unit length of x_{river} for river flow routing consists of overland
 520 flow, lateral subsurface flow, runoff from the river R_{river}^t , and river evaporation loss E_{river}^t , converted to $\text{m}^2 \text{s}^{-1}$. Like the lateral subsurface routing, these equations are solved in wflow_sbm using Newton's method. The number of iterations for surface runoff in the kinematic wave within a time step t , defaults to the Courant number C :

$$C = \frac{c_k dt}{dx}, \quad (90)$$

where c_k [m s^{-1}] is the kinematic wave celerity: $c_k = \frac{1}{\alpha\beta Q^{\beta-1}}$, and x and t as previously defined. The number of iterations
 525 within a time step t is calculated by multiplying the 95th percentile of C (to remove potential very high values (outliers)) for the wflow_sbm model domain with 1.25. The number of iterations can also be fixed to a specific sub time step [s] for both river and overland flow, this is a model setting in the wflow_sbm configuration file. For river cells in wflow_sbm, where overland and river flow can be both present, lateral subsurface and overland flow into the river cell is partitioned based on the land slope of the river cell $c_{\text{land slope,river}}$ [-] and the land slope $c_{\text{land slope,upstream}}$ [-] of the upstream cell:

$$530 \quad f_{\text{to river}} = \frac{c_{\text{land slope,upstream}}}{c_{\text{land slope,upstream}} + c_{\text{land slope,river}}}, \quad (91)$$

$$f_{\text{to land}} = 1 - f_{\text{to river}}, \quad (92)$$

where $f_{\text{to river}}$ [-] is the fraction of lateral subsurface or overland flow from an upstream cell that flows into the river, and $f_{\text{to land}}$ [-] is the fraction of lateral subsurface or overland flow from an upstream cell that flows into the downstream kinematic reservoir of lateral subsurface and overland flow respectively. In case a river cell has the same flow direction as the upstream
 535 cell, $f_{\text{to river}} = 0$, and thus overland and lateral subsurface flow from the upstream cell do not contribute to flow into the river.



2.7 Reservoirs and lakes

2.7.1 Reservoirs

In `wflow_sbm`, reservoirs can be included in the kinematic wave routing for river flow. The first step in the reservoir module is to calculate the storage S_{res}^t [m^3], based on the storage S_{res}^{t-1} at the previous time step, inflow $Q_{\text{in,res}}^t$ [m^3] at time step t ,
 540 average precipitation P_{res}^t [mm] and potential evapotranspiration $E_{\text{pot,res}}^t$ [mm] on the reservoir area A_{res} [m^2] at time step t :

$$S_{\text{res}}^t = S_{\text{res}}^{t-1} + Q_{\text{in,res}}^t + 0.001P_{\text{res}}^t A_{\text{res}} - 0.001E_{\text{pot,res}}^t A_{\text{res}}. \quad (93)$$

Then the storage fraction $f_{\text{res,storage}}^t$ [-] is calculated based on the maximum storage of the reservoir $S_{\text{res,max}}$ [m^3] (above this storage amount water is spilled):

$$f_{\text{res,storage}}^t = \frac{S_{\text{res}}^t}{S_{\text{res,max}}}. \quad (94)$$

545 The minimum release R_{min}^t [m^3] at time step t is based on a sigmoid function, the minimum flow requirement downstream of the reservoir $Q_{\text{min req.}}^t$ [$\text{m}^3 \text{ s}^{-1}$], the target minimum storage fraction (of $S_{\text{res,max}}$) $f_{\text{res,min}}$ [-] and $f_{\text{res,storage}}^t$ at time step t :

$$R_{\text{min}}^t = \min\left(\frac{Q_{\text{min req.}}^t}{1 + e^{-30(f_{\text{res,storage}}^t - f_{\text{res,min}})}}, S_{\text{res}}^t\right), \quad (95)$$

and R_{min}^t is subtracted from the reservoir storage S_{res}^t :

$$S_{\text{res}}^t = S_{\text{res}}^t - R_{\text{min}}^t. \quad (96)$$

550 An additional release R^t [m^3] is calculated when the reservoir storage is above the target maximum storage fraction $f_{\text{res,max}}$ [-], controlled by the maximum release capacity below the spillway $Q_{\text{max,res}}$ [$\text{m}^3 \text{ s}^{-1}$]:

$$R^t = \min(\max(0, S_{\text{res}}^t - (S_{\text{res,max}} f_{\text{res,max}})), \max(0, S_{\text{res}}^t - S_{\text{res,max}}) + Q_{\text{max,res}} t - R_{\text{min}}^t), \quad (97)$$

and R^t [m^3] is subtracted from the reservoir storage S_{res}^t :

$$S_{\text{res}}^t = S_{\text{res}}^t - R^t. \quad (98)$$

555 2.7.2 Natural lakes

As for the reservoirs in `wflow_sbm`, a mass balance approach is used for modelling natural lakes:



$$\frac{S_{\text{lake}}(t + \Delta t)}{\Delta t} = \frac{S_{\text{lake}}(t)}{\Delta t} + Q_{\text{in,lake}} + \frac{0.001(P_{\text{lake}} - E_{\text{lake}})A_{\text{lake}}}{\Delta t} - Q_{\text{out,lake}}. \quad (99)$$

where S_{lake} is lake storage [m^3], Δt is the model timestep [s], $Q_{\text{in,lake}}$ is the sum of inflows [$\text{m}^3 \text{ s}^{-1}$], $Q_{\text{out,lake}}$ is the lake outflow at the outlet [$\text{m}^3 \text{ s}^{-1}$], P_{lake} is precipitation [mm], E_{lake} is lake evaporation [mm] and A_{lake} is the lake surface [m^2].
 560 Most of the terms in Eq. (99) are known at the current or previous time step, except $S_{\text{lake}}(t + \Delta t)$ and $Q_{\text{out,lake}}$. For lakes characterized by a storage curve of the form $S_{\text{lake}} = A_{\text{lake}}H_{\text{lake}}$ and the following rating curve:

$$Q_{\text{out,lake}} = \alpha(H_{\text{lake}} - H_{0,\text{lake}})^\beta, \quad (100)$$

where $H_{0,\text{lake}}$ is the minimum water level under which the outflow is zero, and the β exponent has a value of 2 (parabolic weir) the Modified Puls Approach is used. Then, S_{lake} can be expressed as follows:

$$565 \quad S_{\text{lake}} = A_{\text{lake}}H_{\text{lake}} = A_{\text{lake}}(h + H_{0,\text{lake}}) = \frac{A_{\text{lake}}}{\sqrt{\alpha}}\sqrt{Q_{\text{out,lake}}} + A_{\text{lake}}H_{0,\text{lake}}. \quad (101)$$

Inserting this equation in the mass balance equation gives:

$$\frac{A_{\text{lake}}}{\Delta t\sqrt{\alpha}}\sqrt{Q_{\text{out,lake}}} + Q_{\text{out,lake}} = \frac{S_{\text{lake}}(t)}{\Delta t} + Q_{\text{in,lake}} + \frac{0.001(P_{\text{lake}} - E_{\text{lake}})A_{\text{lake}}}{\Delta t} - \frac{A_{\text{lake}}H_{0,\text{lake}}}{\Delta t}. \quad (102)$$

The solution for $Q_{\text{out,lake}}$ is then:

$$Q_{\text{out,lake}} = \begin{cases} \left(-f_{\text{lake}} + \sqrt{f_{\text{lake}}^2 + 2\left(SI_{\text{lake}} - \frac{A_{\text{lake}}H_{0,\text{lake}}}{\Delta t}\right)} \right)^2, & \text{if } SI_{\text{lake}} > \frac{A_{\text{lake}}H_{0,\text{lake}}}{\Delta t}, \\ 0, & \text{if } SI_{\text{lake}} \leq \frac{A_{\text{lake}}H_{0,\text{lake}}}{\Delta t}, \end{cases} \quad (103)$$

$$570 \quad \text{where } f_{\text{lake}} = \frac{A_{\text{lake}}}{\Delta t\sqrt{\alpha}}, \text{ and } SI_{\text{lake}} = \frac{S_{\text{lake}}(t)}{\Delta t} + Q_{\text{in,lake}} + \frac{0.001(P_{\text{lake}} - E_{\text{lake}})A_{\text{lake}}}{\Delta t}.$$

The Modified Puls Approach is not applicable for lakes characterized by a rating curve (Eq. 100) with $\beta \neq 2$ (non-parabolic weir, for a rectangular weir usually a value of 3/2 is used) or a rating curve from measurements (linear interpolation of $Q_{\text{out,lake}}$ and H_{lake} values in a lookup table), in combination with a storage curve from measurements (linear interpolation of S_{lake} and H_{lake} values in a lookup table) or computed from the relationship $S_{\text{lake}} = A_{\text{lake}}H_{\text{lake}}$. For these lakes $Q_{\text{out,lake}}$ is first computed
 575 for each time step, based on H_{lake} at the previous time step. Then, S_{lake} is updated with Eq. (99), and H_{lake} is updated with the storage curve based on the updated S_{lake} . For closely lakes which are connected it is possible to link the lakes and return flow can be allowed from the downstream to the upstream lake. An average lake water level ($H_{\text{lake,avg}}$ [m]) should be provided as an initial state when wflow_sbm is initialized with default values in the code (“cold” start), see also Table A2.



3 Computational performance

580 One of the reasons to switch to the Julia programming language is that it offers high performance, required for large-scale high-resolution hydrologic model applications. Here we compare the simulation times of `wflow_sbm` between the Julia (van Verseveld et al., 2022a) and Python (Schellekens et al., 2020) version, for three large catchments: Moselle, Meuse and Rhine (Fig. 2). We used HydroMT-Wflow (Eilander et al., 2022) to setup the models for the three catchments at a resolution of 30'' (~1km × 1km). The models were run at a daily time step for 5 years (2000-2005) with ERA5 forcing data. We did exclude
585 the I/O operations to allow for a clean comparison between the Julia and Python version, and ran the simulation on a machine with the following specifications: a desktop with an Intel Xeon Gold 6144 CPU (with 4 cores, 4 threads exposed to the user) and 16GB RAM.

The switch to Julia results in substantial smaller simulation times, independent of the size of the catchment (Fig. 2). By enabling threads (Julia version) the simulation times decrease further, leading to a model that runs 4-5 times faster compared to
590 the Python version. For the Rhine catchment the simulation time for 1 year is 120 min for the `wflow_sbm` Python version, for the Julia version this is 37 min and 25 min with 1 and 4 threads, respectively. These simulation times take up most of the total computational time (> 98%). These results show that the `wflow_sbm` Julia version is suitable for large-scale high-resolution model applications.

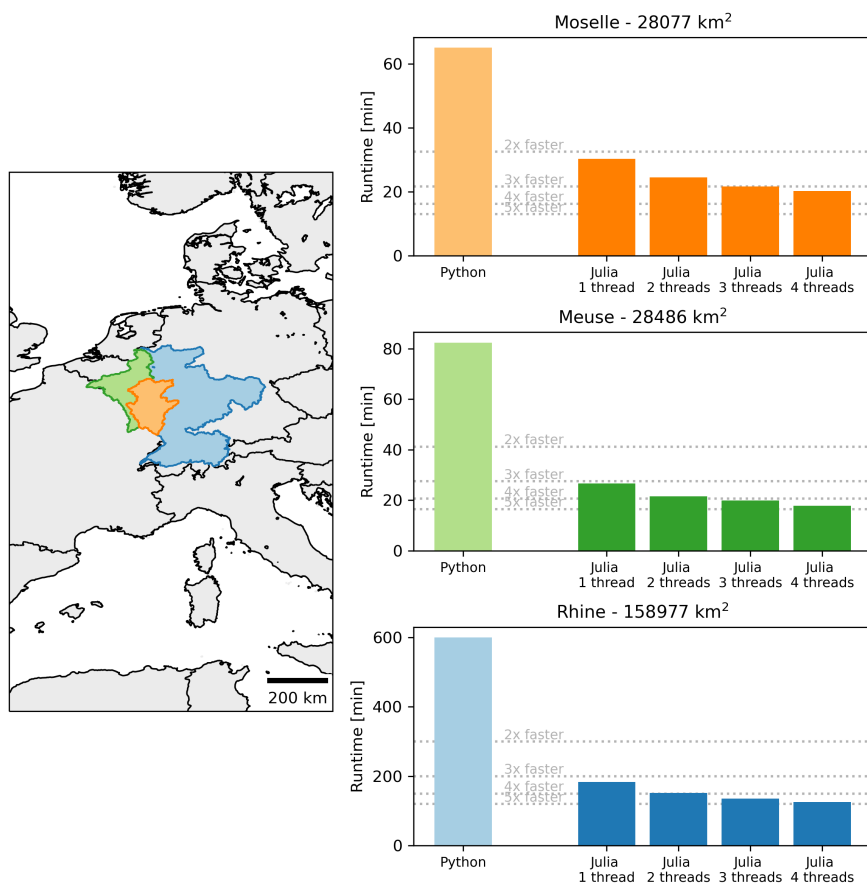


Figure 2. Simulation times of the wflow_sbm model in three large catchments with the wflow Python version 2020.1.2 (Schellekens et al., 2020) and Wflow.jl v0.6.1 (van Verseveld et al., 2022a), including multithreading in the Julia version.

4 Applications

595 The wflow_sbm model has been applied to a number of specific cases. Below we describe these specific applications and its a-priori parameter estimation, including forcing, with HydroMT-Wflow for a variety of hydroclimates and hydrological processes.

4.1 Parameter estimation with HydroMT-Wflow

600 The estimation of wflow_sbm model parameters is based on earlier work by Imhoff et al. (2020) that focused on the Rhine basin, and the development of the Iterative Hydrography Upscaling (IHU) method by Eilander et al. (2021) to derive flow direction and representative river length, slope and width parameters. Eilander et al. (2021) showed an improved accuracy with IHU upscaled flow direction maps, applied to MERIT Hydro, compared to other often-used upscaling methods. Furthermore, for a case study



of the Rhine basin, Eilander et al. (2021) showed that with IHU applied to MERIT Hydro, errors in the timing and magnitude of simulated peak discharge compared to simulations at the native data resolution are minimized. Imhoff et al. (2020) used available point-scale (pedo)transfer-functions (PTFs) from literature to generate seamless parameter maps for the Rhine basin. Following the Multiscale Parameter Regionalization (MPR) technique (Samaniego et al., 2010), parameters were estimated on the original data resolution ('level-0'), and upscaled to the model resolution ('level-1') with upscaling operators. Although universal scaling rules for hydrological model parameters are not available, the correct upscaling operator is found when model parameters are characterized by a constant mean and standard deviation across different spatial resolutions. Additionally, model fluxes and states should be consistent across different spatial resolutions. For the Rhine basin, Imhoff et al. (2020) found that modelled actual evapotranspiration fluxes were consistent across different spatial resolutions (1.2, 2.4, 3.6, and 4.8 km). Routed discharge in headwater basins was not consistent across scales (KGE decreased from the finest to the coarsest resolution), while for the main Rhine river routed discharge was consistent. For recharge fluxes, relatively large differences were found for regions with high drainage densities.

The transfer function and upscaling operators to derive `wflow_sbm` model parameters for any region in the world are part of the HydroMT-Wflow software (Eilander et al., 2022) and are listed in Table 1. For two sensitive `wflow_sbm` model parameters, the temperature threshold ($s_{\text{fall}, T_{\text{threshold}}}$) and the multiplication factor $f_{K_{h0}}$, a PTF is not available (Imhoff et al., 2020). For $s_{\text{fall}, T_{\text{threshold}}}$ and $f_{K_{h0}}$ a uniform default value of 0.0 °C and 100.0 is applied (Table 2), respectively. The a-priori parameter estimation for `wflow_sbm` provides a model setup without the need for much further calibration, in most cases only the model parameter $f_{K_{h0}}$ is tuned (e.g., Wannasin et al., 2021a; Sperna Weiland et al., 2021).

Table 1 also includes references to examples of global datasets that can be used to set up a `wflow_sbm` model with HydroMT-Wflow. For soil properties the SoilGrids (Hengl et al., 2017) at 250 m resolution is available. For land cover the datasets GlobCover-2009 (Arino et al., 2010) at 300 m resolution, VITO v2.0.2 (Buchhorn et al., 2019) at 100 m resolution and Corine Land Cover (CLC) 2018 (European Environment Agency, 2018) are currently available. Leaf area index climatology is based on the MCD15A3H Version 6 Leaf Area Index product, at 500 m resolution (Myneni et al., 2015). For elevation and derived data, the MERIT DEM-based Hydrography map (MERIT Hydro, Yamazaki et al., 2019) at 90 m resolution is used. It contains a global flow direction map derived from the Multi-Error-Removed Improved-Terrain Digital Elevation Model dataset (MERIT DEM, Yamazaki et al., 2017) and a synthetic water layer map that consists of a combination of the Global 1-s Water Body Map (G1WBM, Yamazaki et al., 2015), Global Surface Water Occurrence (GSWO, Pekel et al., 2016) and water-related features from OpenStreetMap. The fine-resolution MERIT Hydro flow direction map is upscaled to the `wflow_sbm` model resolution with the Iterative Hydrography Upscaling (IHU) method (Eilander et al., 2021). River width (w_{river}) and bankfull depth (h_{bankfull}) are based on MERIT Hydro (river mask based on a minimum upstream area) and the global reach-level bankfull river width dataset from Lin et al. (2019). River bankfull depth h_{bankfull} is estimated from bankfull discharge (Q_{bankfull}) data in Lin et al. (2019) with the following power law relationship:

$$h_{\text{bankfull}} = cQ_{\text{bankfull}}^p, \quad (104)$$



with $c = 0.27$ (default) and $p = 0.30$ (default).

For glacier-related model parameters, the Randolph Glacier Inventory 6.0 (Pfeffer et al., 2014) is available. Lake-related parameters are derived from the HydroLAKES Version 1.0 (Messenger et al., 2016) dataset, and reservoir parameters are based on a combination of The Global Reservoir and Dam Database (GRanD), Version 1, Revision 01 (v1.01) (Lehner et al., 2011),
640 HydroLAKES Version 1.0 (Messenger et al., 2016), and GSWO datasets. For more details on the setup of a wflow_sbm model, from global (or regional/local) datasets with HydroMT-Wflow, we refer to the documentation and code of HydroMT-Wflow (Eilander et al., 2022).

Figure 3 shows examples of model parameter maps setup with HydroMT-Wflow for the Moselle catchment (see also section 4.2.4). The parameters are related to elevation (slope), elevation and flow direction (Strahler stream order), land cover (rooting
645 depth) and soil properties (vertical saturated hydraulic conductivity).

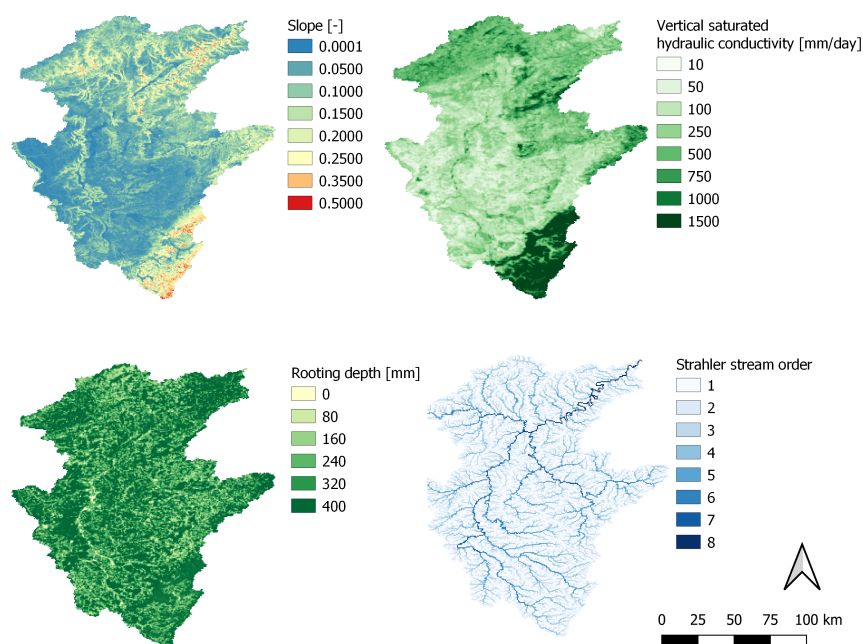


Figure 3. Wflow_sbm static model parameter maps slope, vertical saturated hydraulic conductivity, rooting depth and Strahler stream order for catchment Moselle.

4.2 Wflow_sbm model cases

The wflow_sbm model cases have been setup with HydroMT-Wflow at a resolution of $30''$ based on the (pedo)transfer functions listed in Table 1 and HydroMT-Wflow constant default model parameters listed in Table 2. We present two model cases illustrating the model sensitivity to the model parameter horizontal hydraulic conductivity f_{Kh0} (Whanganui catchment, see
650 section 4.2.1) and the parameter f_{Kv} (Crystal River catchment, see section 4.2.2) that controls the exponential decline of vertical



Table 1. List of wflow_sbm parameters estimated with a (pedo)transfer function (PTF). Upscaling operators are abbreviated as follows: A - arithmetic mean, $\log A$ - arithmetic mean of the natural logarithm.

Parameter	Equation or Section	(pedo)transfer function	Upscaling operator	Additional notes
c	Eq. (46) and (47)	Rawls and Brakensiek (1989) applied to SoilGrids	$\log A$	λ upscaled with $\log A$, c determined from λ at model resolution
k	Eq. (19)	Van Dijk and Bruijnzeel (2001)	A	Lookup table from land cover
K_{vz}, K_{v0}	Eq. (48)	Brakensiek et al. (1984) applied to SoilGrids	$\log A$	For the soil depths z : 0, 5, 15, 30, 60, 100 and 200 cm
LAI	Eq. (18) and (19)	Myneni et al. (2015)	A	LAI climatology from the period 2003-2017
f_{Kv}	Eq. (48)			Fitting exponential function between K_{vz} and z
n_{land}	Eq. (89)	Engman (1986); Kilgore (1997)	A	Lookup table (land cover)
n_{river}	Eq. (89)	Liu et al. (2005)	A	Derived at model resolution, lookup table (Strahler order)
z_{rooting}	Eq. (65)	Schenk and Jackson (2002); Fan et al. (2016)	A	d_{75} rooting depth, lookup table
S_{leaf}	Eq. (18)	Pitman (1989); Liu (1998)	A	Lookup table (land cover)
$c_{\text{land slope}}$	Eq. (82) and (89)	Horn (1981)	A	Derived from MERIT DEM
$c_{\text{river slope}}$	Eq. (89)			Derived from MERIT Hydro
x_{river}	Sect. (2.6)			Derived from MERIT Hydro
w_{river}	Sect. (2.6)	Lin et al. (2019)		River mask from MERIT Hydro
h_{bankfull}	Sect. (2.6)	Lin et al. (2019)		River mask from MERIT Hydro
z_{soil}	Eq. (38)	Hengl et al. (2017); ESDAC (2004)	A	
$S_{\text{wood,max}}$	Sect. (2.2.3)	Pitman (1989); Liu (1998)	A	Lookup table (land cover)
θ_s	Eq. (38)	Tóth et al. (2015)	A	
θ_r	Eq. (38)	Tóth et al. (2015)	A	
$f_{\text{open water}}$	Eq. (55)		A	Lookup table (land cover)
f_{paved}	Sect. (2.4.1)		A	Lookup table (land cover)
$S_{\text{glacier}}, f_{\text{glacier}}$	Eq. (34)	Pfeffer et al. (2014)		
$H_{\text{lake,avg}}, \alpha, A_{\text{lake}}$	Sect. (2.7.2)	Messenger et al. (2016)		Lake parameters, fixed $\beta = 2$
$A_{\text{res}}, S_{\text{res}}, f_{\text{res,min}}, f_{\text{res,max}}, Q_{\text{min req.}}, Q_{\text{max,res}}$	Sect. (2.7.1)	Lehner et al. (2011); Messenger et al. (2016); Pekel et al. (2016)		Reservoir parameters



Table 2. Constant wflow_sbm model parameter values defined in HydroMT-Wflow (Eilander et al., 2022).

Parameter	Equation	Value
$\frac{E_{sat}}{P_{sat}}$	Eq. (1)	0.11
$C_{infiltration,paved}$	Eq. (43)	5.0 mm day ⁻¹
$C_{infiltration,unpaved}$	Eq. (42)	600.0 mm day ⁻¹
$f_{red,frozen}$	Eq. (40)	0.038
$s_{fall,Tthreshold}$	Eq. (20)	0.0 °C
$s_{fall,Tinterval}$	Eq. (20)	2.0 °C
s_{ddf}	Eq. (23) and (24)	3.75653 mm °C ⁻¹ day ⁻¹
$s_{melt,Tthreshold}$	Eq. (23) and (24)	0.0 °C
s_{whc}	Eq. (27)	0.1
g_{ddf}	Eq. (32)	5.3 mm °C ⁻¹ day ⁻¹
$g_{snow\ to\ ice}$	Eq. (30)	0.002
$g_{melt,Tthreshold}$	Eq. (32)	1.3 °C
C_{rd}	Eq. (65)	-500.0
f_{Kh0}	Eq. (82)	100.0
L_{max}	Eq. (81)	0.0 mm day ⁻¹

saturated hydraulic conductivity. We also illustrate how wflow_sbm performs based on the a-priori parameter estimation with only changing the model parameter f_{Kh0} for the catchment Umeälven (section 4.2.3), where reservoir operations and snow processes play an important role, and for the Moselle catchment (section 4.2.4) including discharge and soil moisture as output. Finally, we present a model case for the Oueme catchment (section 4.2.5), where groundwater loss plays an important role.

655 The location of the wflow_sbm model cases on a global map are shown in Fig. 4a. For each model case a map of the catchment with elevation and rivers is presented in Fig. 4b-f. For each model case four soil layers are defined as follows (default): 0-10, 10-40, 40-120 and 120 cm up till the maximum soil depth z_{soil} (Table 1), to capture changes in soil hydraulic properties and roots, and thus soil moisture fluxes, with depth. Wflow_sbm determines the actual soil layer thickness for each layer per grid cell based on z_{soil} . For river and overland flow the time step is set to a fixed value of 900 and 3600 s, respectively.

660 is enabled, a reduction factor to infiltration in soils because of frozen conditions, is not applied. Other, more specific model settings are described per model case in sections 4.2.1 - 4.2.5.

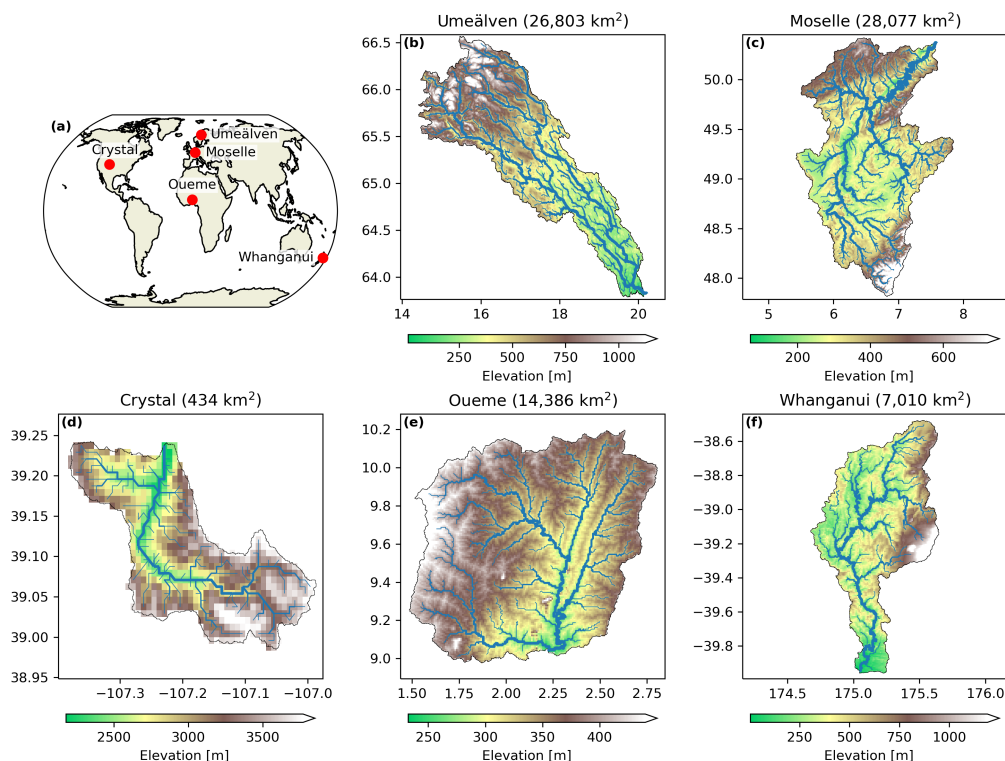


Figure 4. Locations and maps of wflow_sbm model cases: (a) model case locations on a global map, (b) Europe - Umeälven (section 4.2.3), (c) Europe - Moselle (section 4.2.4), (d) USA - Crystal River (section 4.2.2), (e) Africa - Oueme River (section 4.2.5), (f) New Zealand - Whanganui River (section 4.2.1).

The model performance of the wflow_sbm applications is here assessed with the modified Kling-Gupta Efficiency (KGE, Kling et al., 2012):

$$KGE = 1 - \sqrt{(r - 1)^2 + (\beta - 1)^2 + (\gamma - 1)^2} \quad (105)$$

665 where r is the the correlation coefficient between observed and simulated values, β is a bias term and γ is the variability ratio:

$$KGE = 1 - \sqrt{(r - 1)^2 + \left(\frac{\mu_{sim}}{\mu_{obs}} - 1\right)^2 + \left(\frac{\sigma_{sim}/\mu_{sim}}{\sigma_{obs}/\mu_{obs}} - 1\right)^2} \quad (106)$$

where μ_{sim} is the mean of simulated values, μ_{obs} is the mean of observed values, σ_{sim} is the standard deviation of simulated values and σ_{obs} is the standard deviation of observed values. $KGE = 1$ means a perfect match between simulated and observed values, and $KGE \approx -0.41$ indicates the model simulation is as accurate as the observed mean (Knoben et al., 2019). For each
 670 model case we use the first year as warm-up period. For the simulations of all except two model cases we use ERA5 forcing,



temperature and potential evapotranspiration (using de Bruin method (de Bruin et al., 2016)) are derived based on downscaled ERA5 fields using a fixed lapse rate of $-0.0065 \text{ }^\circ\text{C m}^{-1}$. For the model case of the Crystal River catchment (section 4.2.2) forcing is based on the dataset by Maurer et al. (2002), and for the case of catchment Oueme (section 4.2.5) we use Climate Hazards group Infrared Precipitation with Stations (CHIRPS) rainfall (Funk et al., 2015) estimates instead of ERA5 rainfall.

675 4.2.1 New Zealand - Whanganui River - Effect of model parameter $f_{K_{h0}}$

The wflow_sbm model parameter $f_{K_{h0}}$ is a multiplication factor applied to the vertical saturated hydraulic conductivity at the soil surface K_{v0} to calculate the horizontal saturated conductivity used for computing lateral subsurface flow. This parameter compensates for anisotropy, small scale saturated hydraulic conductivity (soil core) measurements that do not represent larger scale hydraulic conductivity, and smaller flow length scales (hillslope) in reality, not represented by the model resolution. Land
680 cover derived model parameters are based on VITO v2.0.2 (Buchhorn et al., 2019). For this model case, the snow (including the snow avalanche routine) and glacier model are enabled. To illustrate the effect of different $f_{K_{h0}}$ values (1, 20, 50, 100), Fig. 5 shows the discharge simulation (daily time step) and KGE values for GRDC station 5865600 of the Whanganui River catchment in New Zealand, for the year 1996. Figure 5 clearly shows that higher $f_{K_{h0}}$ values results generally in higher baseflow values and flattened peaks. The $f_{K_{h0}}$ value of 20 results in the highest KGE of 0.71 for the year 1996. For the complete period of
685 simulation 1979-2009, the KGE values were 0.63, 0.79, 0.68 and 0.55 for $f_{K_{h0}}$ values 1, 20, 50 and 100, respectively.

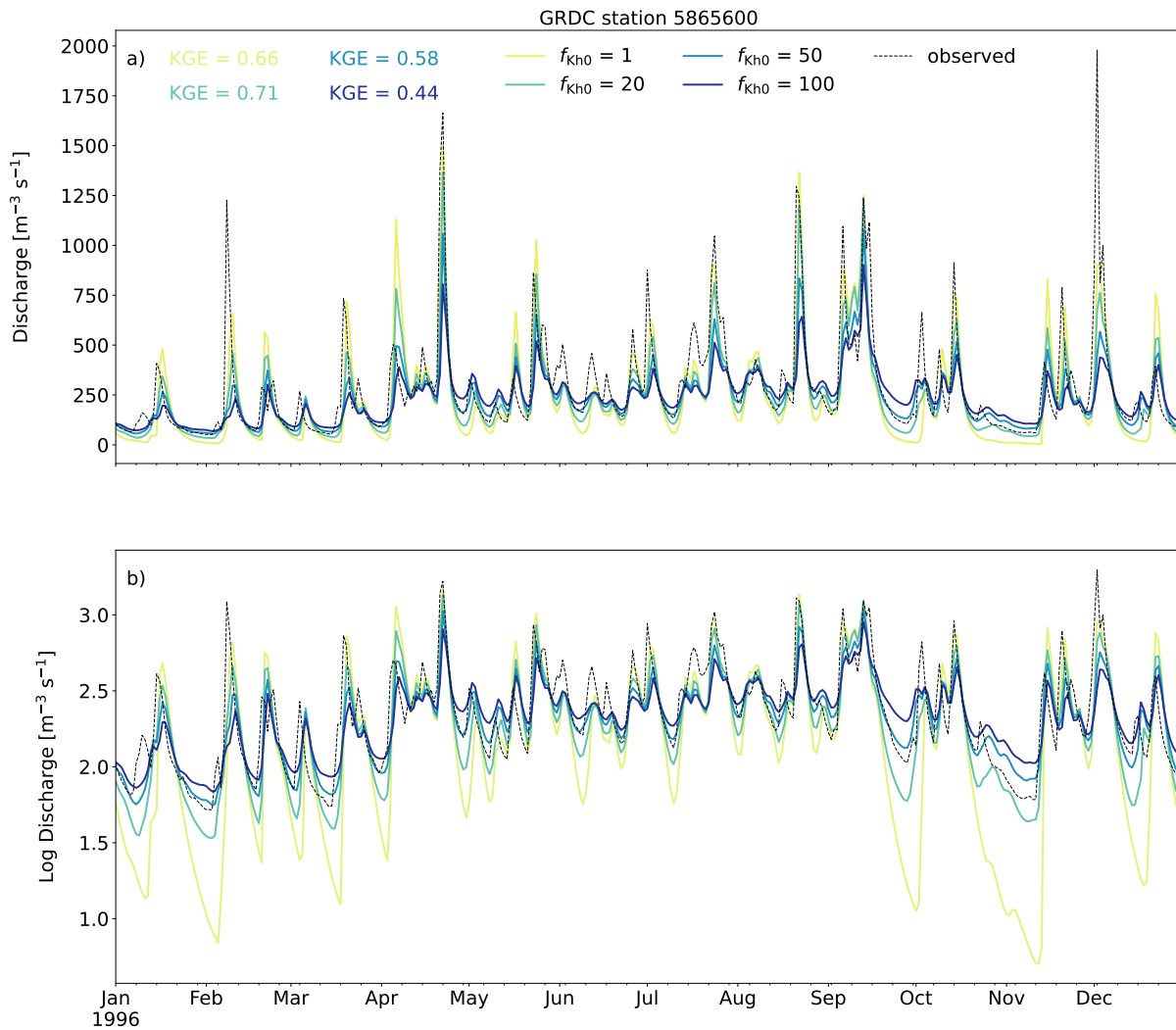


Figure 5. Effect of f_{Kh0} on simulated discharge for GRDC station 5865600 of the Whanganui River catchment, in 1996. (a) discharge, (b) \log_{10} of the discharge.

By changing the parameter f_{Kh0} it is expected that the contribution of overland flow and lateral subsurface flow to river discharge will change. We show in Fig. 6a the effect of different f_{Kh0} values (1 and 100) on the average lateral inflow components subsurface flow $Q_{\text{subsurface,to river}}$ and overland flow $Q_{\text{land,to river}}$ to the river. With a f_{Kh0} value of 1, the contribution of $Q_{\text{subsurface,to river}}$ is minimal, and river inflow consists mainly of $Q_{\text{land,to river}}$, with high values during discharge peaks and quickly dropping to low values during baseflow conditions (Fig. 6a). The average water table depth $z_{\text{watertable}}$ is low without much variation with a f_{Kh0} value of 1 (Fig. 6b). With a f_{Kh0} value of 100, the contribution of $Q_{\text{subsurface,to river}}$ is higher, and $Q_{\text{land,to river}}$ is lower during peaks and higher during baseflow conditions, compared to a f_{Kh0} value of 1. On average $z_{\text{watertable}}$ is lower and shows more variation with a f_{Kh0} value of 100 compared to a f_{Kh0} value of 1 (Fig. 6b). Thus,



695 $f_{K_{h0}}$ controls the distribution of $Q_{\text{subsurface,to river}}$ and $Q_{\text{land,to river}}$, related to the overall wetness of the catchment and the magnitude of lateral subsurface flows ($Q_{\text{subsurface}}$), which has an effect on the peak discharges and baseflow values of the hydrograph.

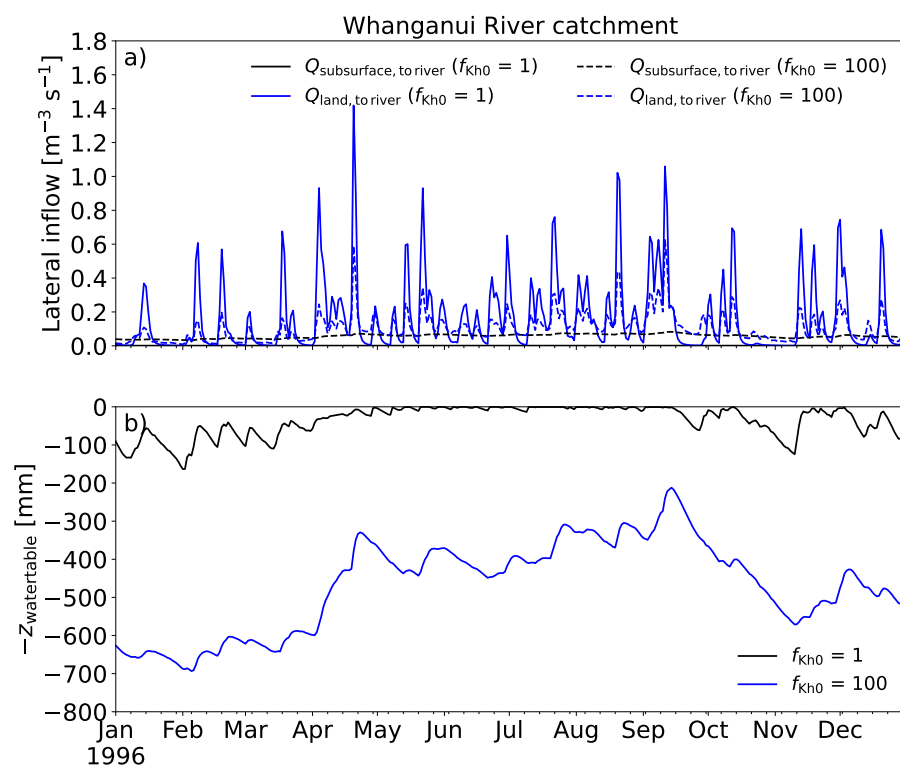


Figure 6. Simulated (a) average lateral inflow (subsurface flow $Q_{\text{subsurface,to river}}$ and overland flow $Q_{\text{land,to river}}$), (b) average water table depth $z_{\text{watertable}}$, of the Whanganui River catchment, in 1996, with $f_{K_{h0}} = 1$ and $f_{K_{h0}} = 100$.

4.2.2 USA - Crystal River - Effect of exponential decline of K_{v0}

The wflow_sbm parameter f_{K_v} controls the exponential decline of the vertical saturated hydraulic conductivity K_{v0} at the soil surface with depth, and thus vertical flow and lateral subsurface flow. A-priori, f_{K_v} is estimated with HydroMT-Wflow through the use of two different fitting methods using non-linear least squares (curve_fit) and a least-squares solution (linalg.lstsq) applied to the estimated vertical saturated hydraulic conductivity K_{vz} at different depths from SoilGrids (see also Table 1). Figure 7 shows simulated (daily time step) discharge for the Crystal River near Redstone (Colorado, USA) in 2003, with land cover derived model parameters based on VITO v2.0.2 (Buchhorn et al., 2019). For this model case, the snow (including the snow avalanche routine) model is enabled. For both fitting methods the performance is good (KGE 0.9 or higher), the fitting method using non-linear least squares (curve_fit) result in a higher KGE value. This fitting method is capturing the rising limb (partially caused by snow melt) during the period 15 March - 15 May, and generally the falling limb (less overestimation) of



the hydrograph better. The average f_{K_v} value for the catchment was 0.0027 and 0.0011 for fitting using non-linear least squares and least-squares solution, respectively. A higher f_{K_v} value results in a more exponential decline of K_{v0} with depth.

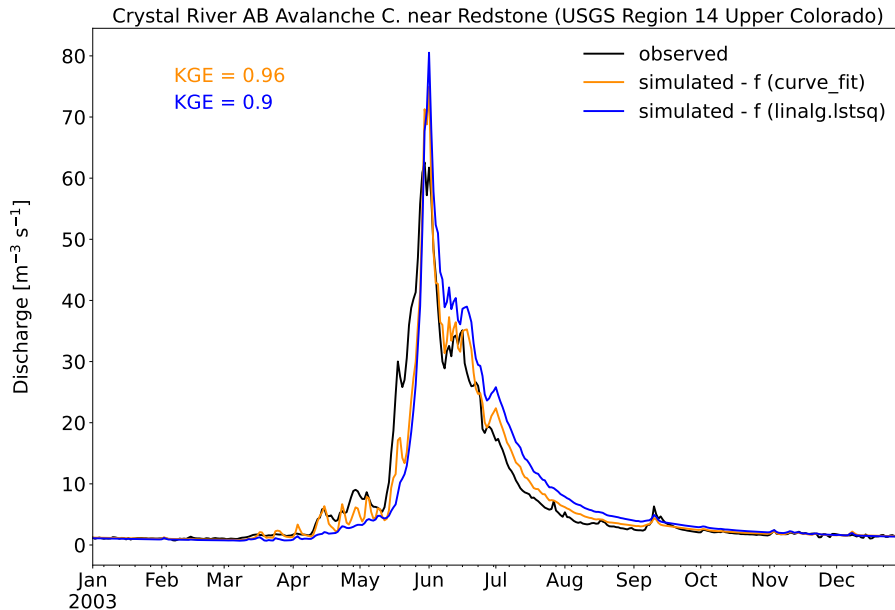


Figure 7. Simulated discharge for the Crystal River near Redstone (Colorado, USA) in 2003, with different fitting methods for f_{K_v} .

As for the parameter $f_{K_{h0}}$, it is expected that by changing the f_{K_v} parameter the contribution of overland flow and lateral
710 subsurface flow to river discharge will change. We show the effect of the different f_{K_v} values as a result of different fitting
methods on the average lateral inflow components $Q_{\text{subsurface,to river}}$ and $Q_{\text{land,to river}}$ to the river in Fig. 8a, and on $z_{\text{watertable}}$
in Fig. 8b. The `curve_fit` fitting method is capturing the rising limb of the hydrograph better during the period 15 March - 15
715 May because the contribution of $Q_{\text{land,to river}}$ is higher compared to the `linalg.lstsq` fitting method, while the $Q_{\text{subsurface,to river}}$
contribution is similar (Fig. 8a). With the `curve_fit` fitting method the catchment is wetter; $z_{\text{watertable}}$ has a shallower pattern
compared to the `linalg.lstsq` fitting method (Fig. 8b), causing higher $Q_{\text{land,to river}}$ values. During the falling limb of the hydro-
graph, the `curve_fit` fitting method results in less overestimation caused by a lower $Q_{\text{subsurface,to river}}$ contribution, while the
 $Q_{\text{land,to river}}$ contribution is similar (Fig. 8a).

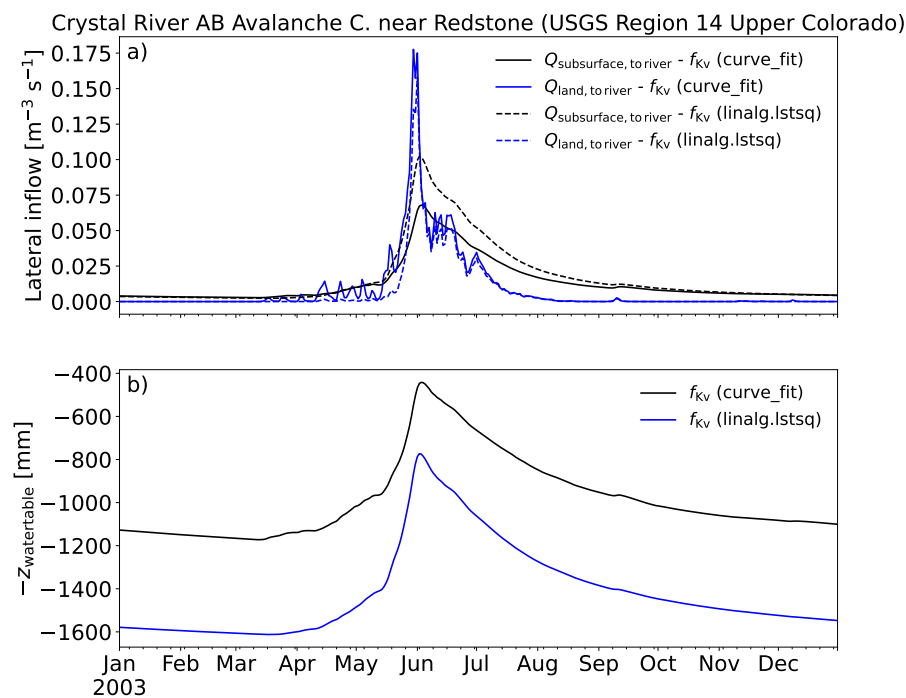


Figure 8. Simulated (a) average lateral inflow (subsurface flow $Q_{\text{subsurface, to river}}$ and overland flow $Q_{\text{land, to river}}$), (b) average water table depth $z_{\text{watertable}}$, for the Crystal River near Redstone (Colorado, USA) in 2003, with different fitting methods for f_{Kv} .

4.2.3 Europe - Umeälven - Snow and Reservoirs

The Ume river in Sweden is one of the largest rivers in Sweden and has been extensively cultivated for hydroelectric power. From a hydrometeorological aspect, snowfall and melt play here an important role. Furthermore, accounting for these hydropower stations in the hydrological model is done on the basis of the information in the GRanD, HydroLAKES and GWSO datasets. This information is rather uncertain as hydropower operators have their own release curves or optimization schemes. Here, we simulated discharge for the period 1979 until 2020 at a daily time step, with land cover derived model parameters based on CLC 2018 (European Environment Agency, 2018). The values derived for the vertical hydraulic conductivity are quite large in the order of a few meters per day and hence no anisotropy factor for lateral hydraulic conductivity was applied ($f_{K_{h0}} = 1$). For this model case, the snow (including the snow avalanche routine) and glacier model are enabled, and lakes and reservoirs are included.

Figure 9 presents KGE scores for Swedish Meteorological and Hydrological Institute (SMHI) stations simulated with E-HYPE (Swedish Meteorological and Hydrological Institute, 2022) and wflow_sbm. Observed discharges for the stations were obtained from Swedish Meteorological and Hydrological Institute (2021). Because of differences in forcing, simulation periods and the use of different KGE methods, a quantitative comparison of model performance scores is not possible. However, it is obvious that for locations (20010 and 20047) largely influenced by reservoirs and lakes, and thus reservoir operations, both



models show poor performance. For a more upstream location like 1630, E-HYPE performance is good ($KGE > 0.8$) and wflow_sbm performance is satisfactory ($KGE = 0.66$). Wflow_sbm shows lower KGE values for locations 2237 and 2238, while for locations 1733 and 1734 wflow_sbm shows a better performance. Wflow_sbm performance for the unregulated Vindel river (locations 1630, 2237 and 2238), a tributary to the Ume river, could probably be improved on the basis of E-HYPE performance. This could be done for example through a further analysis of the impact of different snow model parameters like $s_{fall, T_{threshold}}$ and s_{ddf} on model performance, lake model settings of lake Storovan, and possibly other forcing datasets than ERA5.

Figure 10 shows simulated and observed discharge for the SMHI stations within catchment Umeälven for the year 1993. The performance for the most downstream stations 1733 and 1734 is satisfactory. The underestimation of discharge peaks for station 1733 during July and August is mostly caused by underestimating discharge peaks at station 20010 (downstream of lake Storuman) during the same period. The actual release scheme of lake Storuman is very likely not captured well enough by wflow_sbm. Wflow_sbm is overestimating baseflow and underestimating peak flows for station 2238 (Fig. 10), downstream of lake Storovan. This may be caused for example by the lake model settings of lake Storovan, upstream model parameters related to lateral subsurface flow (see also sections 4.2.2 and 4.2.1) or snow dynamics, and has an effect on underestimating peak flows at the downstream station 1734 by wflow_sbm. Overall, we show that with the a-priori parameter estimation, the performance for catchment Umeälven is (qualitatively) similar to the E-HYPE performance for this catchment.

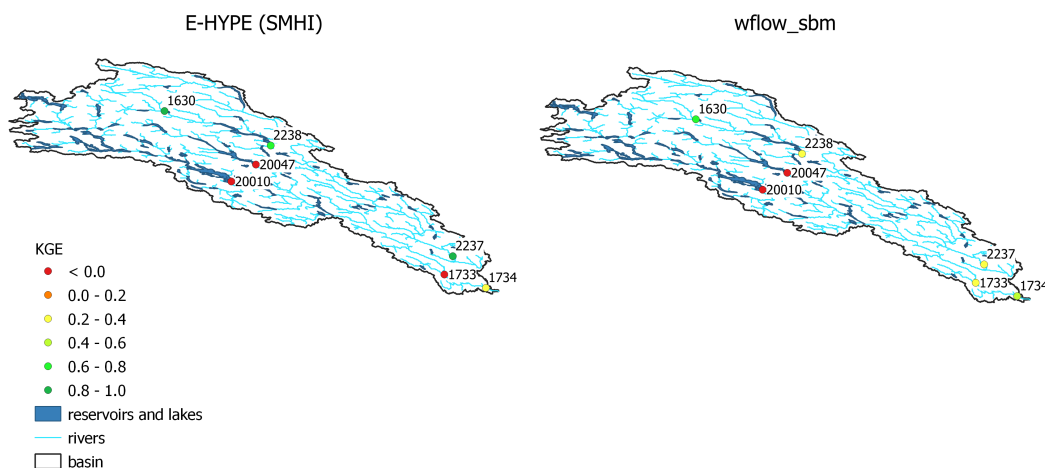


Figure 9. KGE scores for stations within the Umeälven catchment with E-HYPE and wflow_sbm. E-HYPE and wflow_sbm performance is assessed with KGE from Gupta et al. (2009) and the modified KGE from Kling et al. (2012), respectively.

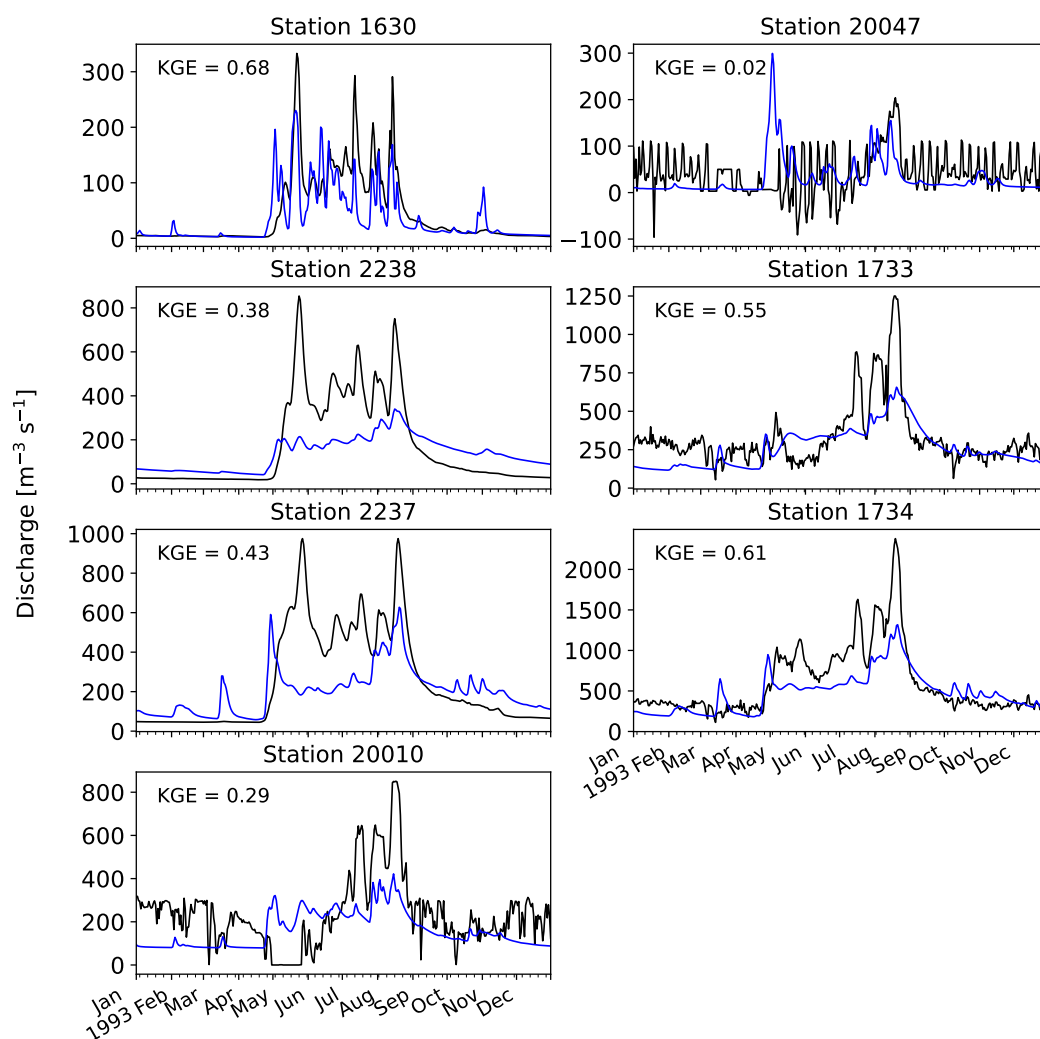


Figure 10. Simulated (blue) and observed discharge (black) for the SMHI stations within catchment Umeälven for the year 1993.

4.2.4 Europe - Moselle - Soil moisture

750 Besides comparing simulated discharge with observed discharge, it can be useful to compare model state variables like soil
moisture or snow water equivalent to actual observations or satellite based datasets for calibration and validation purposes
of the hydrologic model. Here we simulate for the period 1979 until 2020 at a 6-hourly time step, with land cover derived
model parameters that are based on CLC 2018 (European Environment Agency, 2018). We use a f_{Kh0} value of 250 based on
previous hydrologic modelling work of the Rhine basin in Imhoff et al. (2020). For this model case, the snow (including the
755 snow avalanche routine) model is enabled, and lakes and reservoirs are included. The simulated soil moisture dynamics of the
first soil layer (0-10 cm) are compared to the SMAP Enhanced L3 Radiometer dataset (O'Neill et al. , 2021), averaged over the



catchment, for the period 2015 until 2020. Figure 11 shows that wflow_sbm captures the average soil moisture dynamics quite well, with a KGE score of 0.86. Some of the lower and higher soil moisture values of the SMAP Enhanced L3 Radiometer dataset are not captured by wflow_sbm. This could be caused by using the default first soil layer thickness of 10 cm here, while the SMAP Enhanced L3 Radiometer dataset represents the top 5 cm of the soil column. Additionally, differences in used saturated and residual water contents between wflow_sbm and SMAP Enhanced L3 Radiometer can also play a role, for example the average saturated and residual water content for the wflow_sbm model is 0.44 and 0.17 respectively, while the SMAP soil moisture product shows values outside of this range (Fig. 11). Figure 12 shows simulated and observed daily discharge for GRDC station 6336050 (Cochem, near the outlet of the Moselle river in to the Rhine river), for the period 2007-2008, with a KGE score of 0.74. The KGE score for GRDC station 6336050 for the complete simulation period is 0.71, and thus the overall performance of simulated soil moisture dynamics and discharge at the catchment scale is good.

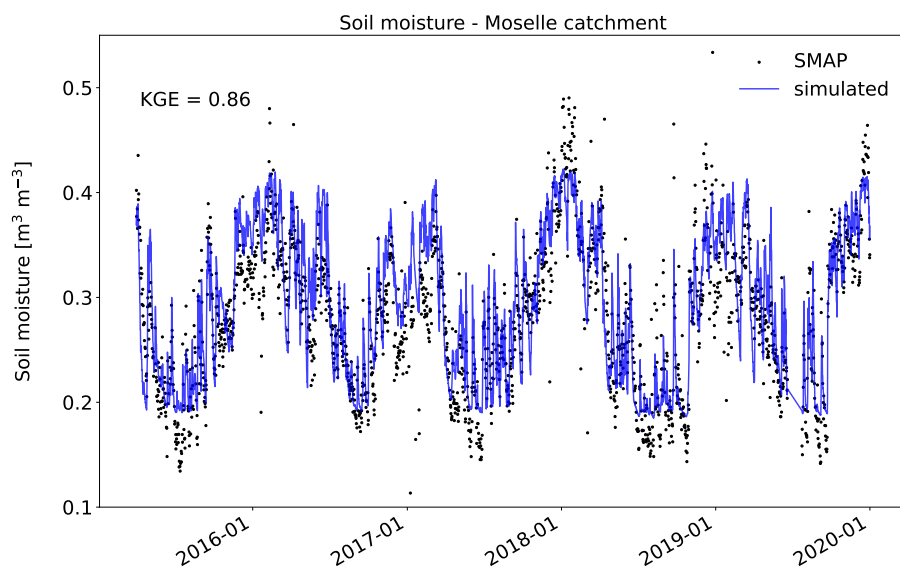


Figure 11. Average simulated and SMAP soil moisture for the Moselle catchment.

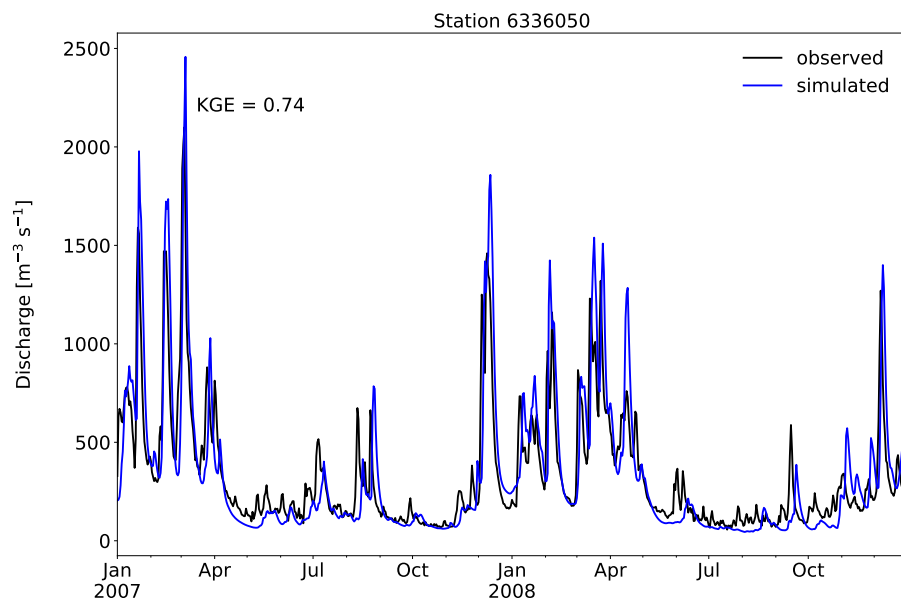


Figure 12. Simulated and observed discharge for GRDC station 6336050 (Cochem).

4.2.5 Africa - Oueme River - groundwater loss

The Oueme mesoscale site (Benin), Africa, is part of the AMMA-CATCH observation network covering a 14,000 km² basin in Sudanian climate on a crystalline basement. It is an interesting test case for wflow_sbm and the automated model setup including a-priori estimation of the model parameters. Various studies using a variety of hydrological model concepts, including similar model concepts as wflow_sbm have been conducted (see Cornelissen et al. (2013) and references therein) for this area. Séguis et al. (2011) reported that around 15% of water is being lost to the groundwater which is disconnected from the river system. Here, we run the wflow_sbm model for the period 1981 until 2020 at a daily time step both without and with groundwater loss ($L_{\max} = 0$ mm/d vs $L_{\max} = 0.6$ mm/d (15% of ~ 4 mm/day of yearly average rainfall)) and analyse the model results for a variety of locations. Land cover derived model parameters are based on VITO v2.0.2 (Buchhorn et al., 2019). For this model case the snow model is disabled, and lakes and reservoirs are not included. Figure 13 shows the KGE scores for the stations within the Oueme mesoscale site without and with groundwater loss. Generally the performance of wflow_sbm increases with groundwater loss with a median increase of 0.86 for all stations. Figure 14 shows simulated discharge for station TEBOU for 2010 with and without groundwater loss. The simulation with groundwater loss clearly shows less overestimation of discharge during the rising limb and peaks of the hydrograph, also reflected in the higher KGE score for the simulation with groundwater loss.

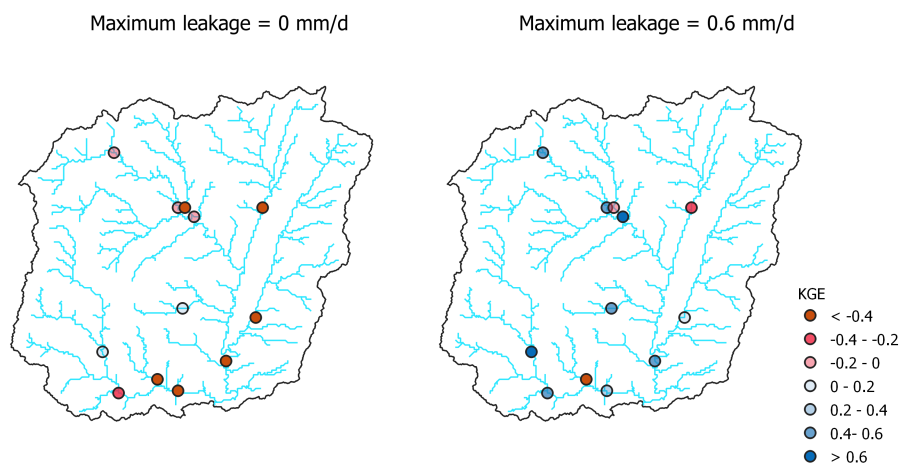


Figure 13. KGE scores for stations within the Oueme mesoscale site without and with groundwater loss.

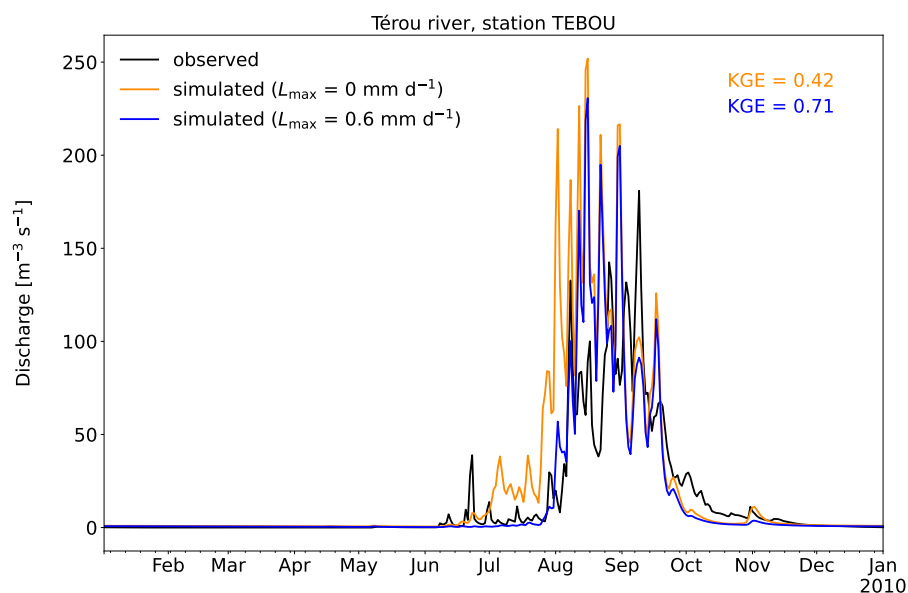


Figure 14. Simulated (with and without groundwater loss) and observed discharge for station TEBOU for 2010.

5 Conclusions and future work

We presented the wflow_sbm hydrological model as part of the Wflow.jl (v0.6.1) open-source modelling framework for distributed hydrologic modelling in Julia, a continuation of the wflow development in the PCRaster-Python framework. Wflow_sbm has been applied in various catchments around the world with satisfactory to good performance. With wflow_sbm we aim to strike a balance between low-resolution, low-complexity and high-resolution, high-complexity hydrologic models. Most



wflow_sbm parameters are based on physical characteristics and at the same time wflow_sbm has a run time performance well suited for large-scale high-resolution modelling. We demonstrated some examples of wflow_sbm applications with Wflow.jl (v0.6.1), using HydroMT-Wflow to setup the wflow_sbm model, including forcing, in an automated way. The wflow_sbm applications illustrate that the a-priori model parameter estimates in combination with a manual adjustment of the f_{Kh0} model parameter result in generally satisfactory to good performance, with for catchment Umeälven similar performance (qualitatively) to E-HYPE. The Oueme River case illustrates the use of the model parameter L_{max} (maximum leakage) based on data from literature, resulting in an overall significant increase in model performance. Including the process of leakage to deeper groundwater results in loss of water outside of the model domain, and we recommend to include this process only if scientific literature or geological data indicate that leakage to deeper groundwater is of importance. With the a-priori parameter estimation, a working wflow_sbm model is setup quickly and incorrect process representations become apparent. The results, e.g. for the Oueme River, indicate that local information and literature studies can help in improving process representation and if not, it opens the way for a better focus on the missing process representation. This is something that lacks when a hydrologic model would directly be calibrated for a given catchment.

While (pedo)transfer function are available for most of the sensitive wflow_sbm model parameters, this is not the case for the f_{Kh0} model parameter. An interesting approach, as part of future work focusing on model data, could be to develop a transfer function for this model parameter by estimating the transfer function with function space optimization (FSO), a method presented by Feigl et al. (2020). Relevant hydrologic processes as glacier and snow processes, evapotranspiration processes, unsaturated zone dynamics, (shallow) groundwater, surface flow routing including lakes and reservoirs are part of wflow_sbm. Floodplain dynamics (backwater effects and floodplain storage) are not part of the kinematic wave routing in Wflow.jl and and this may be problematic to accurately simulate discharge and water depths when backwater effects and floodplain storage cannot be ignored (e.g. Zhao et al., 2017). Additionally, the kinematic wave approach is mostly applicable when slopes are steep and less reliable for low gradient rivers. A recent wflow_sbm development, which is part of v0.6.1, is the improvement of the routing scheme for river-floodplain dynamics and to improve discharge and water depth estimates for low gradient rivers. The improved routing scheme consists of a 1-D local inertial solution for river channel flow and a 2-D local inertial solution for floodplain and overland flow, similar to Neal et al. (2012). Future possible developments related to the improved local inertial routing scheme are 1) improve the multi-threaded performance, 2) vector based routing (e.g. Mizukami et al., 2021) would allow for more flexible channel routing configurations that are less computationally intensive and 3) to combine different routing solutions (e.g. kinematic wave and local inertial) at the submodel-domain scale (e.g. local inertial for the flood plain). For water resources modelling studies, wflow_sbm is often linked to a network-based water allocation model (e.g., Meijer et al., 2021). The development of a water demand module (irrigation, livestock, industrial and domestic) and water allocation module is foreseen, to fully exploit the gridded capabilities of wflow_sbm. The standard soil column of wflow_sbm extends to 2 m below surface level based on SoilGrids data, and although the soil column depth can be increased, the process modelled by wflow_sbm consists of shallow lateral subsurface flow, with an exponential decline of K_{v0} with depth, that may not be appropriate for simulating deep groundwater. While for many applications deep groundwater processes can be ignored, for the coupling with a groundwater model like MODFLOW, or for the extraction of groundwater as part of the foreseen water



demand and allocation developments, implementation of a deep groundwater concept is important. Finally, speedup of the wflow code is ongoing work, recently multi-threading (single node) was added to the wflow code, and further development of distributed computing with a focus on multi-node parallelism using Message Passing Interface (MPI) is planned. In view of these future developments and the current status of the Wflow.jl framework, we have developed the wflow_sbm model which is applicable worldwide, and serves as an important tool to provide relevant information for operational and water resources planning challenges.

Code and data availability. Wflow.jl is open-source and distributed under the terms of the MIT license. The code and documentation is provided through the following GitHub repository <https://github.com/Deltares/Wflow.jl>. Wflow v0.6.1 is available through <https://github.com/Deltares/Wflow.jl/releases/tag/v0.6.1>, Zenodo with the associated DOI: <https://doi.org/10.5281/zenodo.6490936> (van Verseveld et al., 2022a), and is available as a Julia package. The wflow_sbm model cases presented in this paper are available at Zenodo with the associated DOI: <https://doi.org/10.5281/zenodo.6821468> (van Verseveld et al., 2022b). Development and maintenance of Wflow.jl is conducted by Deltares and we welcome contributions from external parties.

Appendix A

A1

A2

Author contributions. WV and MV wrote the majority of the source code and JB, HB, DE, LB and MH contributed to the software development and documentation. WV wrote the original draft of the paper. AW, RI and WV did setup and analyse the model simulations and wrote section 4.2. JB wrote section 3 and produced Fig. 2. LB produced Fig. 1 (adapted from van Verseveld et al. (2022a)). All co-authors contributed to review and editing of the original draft paper.

Competing interests. The authors declare that there is no conflict of interest.

Acknowledgements. This work has received funding from the EU Horizon 2020 Program for Research & Innovation, under grant agreement no 776613 (EUCP: European Climate Prediction system; <https://www.eucp-project.eu>) and from the European High-Performance Computing Joint Undertaking (JU) under grant agreement No 955648 (ACROSS, <https://www.acrossproject.eu/>). The research was co-funded by the Deltares Strategic Research Programs Natural Hazards and Real-Time Information.



Table A1. Wflow_sbm state and flux variables (non-exhaustive).

Symbol	Description	Unit	Wflow.jl name
S_{canopy}	Canopy storage	mm	canopystorage
S_{snow}	Snow storage	mm	snow
$S_{\text{snow,liquid}}$	Amount of liquid water in the snow pack	mm	snowwater
S_{glacier}	Glacier storage	mm	glacierstore
$S_{\text{unsat},n}$	Amount of water in the unsaturated zone, for layer n	mm	ustorelayerdepth
S_{sat}	Amount of water in saturated store	mm	satwaterdepth
S_{res}	Storage of reservoir	m^3	volume
S_{lake}	Lake storage	m^3	storage
H_{lake}	Water level lake	m	waterlevel
P	Precipitation	$\text{mm } t^{-1}$	precipitation
I_{total}	Total interception	$\text{mm } t^{-1}$	interception
$P_{\text{throughfall}}$	Throughfall	$\text{mm } t^{-1}$	throughfall
$F_{\text{available}}$	Water available for infiltration	$\text{mm } t^{-1}$	avail_forinfilt
F_{excess}	Infiltration excess	$\text{mm } t^{-1}$	infiltextcess
$F_{\text{excess,sat}}$	Water that cannot infiltrate due to saturated soil	$\text{mm } t^{-1}$	waterexcess
F_{act}	Actual infiltration	$\text{mm } t^{-1}$	actinfilt
$R_{\text{exfilt,sat}}$	Water exfiltrating during saturation excess conditions	$\text{m } t^{-1}$	exfiltwater
$R_{\text{exfilt,unsat}}$	Water exfiltrating from unsaturated store because of change in water table	$\text{mm } t^{-1}$	exfiltustore
R_{river}	Runoff from river fraction	$\text{mm } t^{-1}$	runoff_river
$R_{\text{open water}}$	Runoff from open water fraction (excluding rivers)	$\text{mm } t^{-1}$	runoff_land
$E_{\text{open water}}$	Evaporation from open water bodies (excluding rivers)	$\text{mm } t^{-1}$	ae_openw_l
E_{river}	Evaporation from rivers	$\text{mm } t^{-1}$	ae_openw_r
$E_{\text{act,sat}}$	Soil evaporation from the saturated store	$\text{mm } t^{-1}$	soilevapsat
$E_{\text{act,soil}}$	Soil evaporation from the unsaturated store	$\text{mm } t^{-1}$	-
$E_{\text{trans,sat}}$	Transpiration from the saturated store	$\text{mm } t^{-1}$	actevapsat
$\sum E_{\text{trans,unsat},n}$	Transpiration from the unsaturated store	$\text{mm } t^{-1}$	ae_ustore
C_{act}	Actual capillary rise	$\text{mm } t^{-1}$	actcapflux
L	Leakage	$\text{mm } t^{-1}$	actleakage
R_{input}	Net recharge to the saturated store	$\text{m } t^{-1}$	recharge
$Q_{\text{subsurface}}$	Subsurface flow	$\text{m}^3 \text{ day}^{-1}$	ssf
$Q_{\text{transfer},n}$	Transfer of water from unsaturated store layer to saturated store	$\text{mm } t^{-1}$	transfer
Q	Surface runoff in the kinematic wave	$\text{m}^3 \text{ s}^{-1}$	q and q_av
$Q_{\text{in,lake}}$	Lake inflow	$\text{m}^3 \text{ s}^{-1}$	inflow
$Q_{\text{out,lake}}$	Lake outflow	$\text{m}^3 \text{ s}^{-1}$	outflow
P_{lake}	Lake average precipitation	$\text{mm } t^{-1}$	precipitation
E_{lake}	Lake average evaporation	$\text{mm } t^{-1}$	evaporation
$Q_{\text{in,res}}$	Reservoir inflow	m^3	inflow
P_{res}	Reservoir average precipitation	$\text{mm } t^{-1}$	precipitation
$E_{\text{pot,res}}$	Reservoir average evaporation	$\text{mm } t^{-1}$	evaporation



Table A2. Wflow_sbm model parameters and forcing.

Symbol	Description	Unit	Wflow_jl name	Default value
P	Precipitation	mm t^{-1}	precipitation	-
$E_{pot, total}$	Potential evapotranspiration	mm t^{-1}	potential_evaporation	-
T_{air}	Air temperature	°C	temperature	-
z_{soil}	Soil depth	mm	soilthickness	2000.0
θ_s	Saturated soil water content	mm mm^{-1}	θ_s	0.6
θ_r	Residual soil water content	mm mm^{-1}	θ_r	0.01
f_{paved}	Fraction of compacted soil (or paved)	-	pathfrac	0.01
$f_{openwater}$	Open water body fraction (excluding rivers)	-	waterfrac	0.0
$c_{infiltration, unpaved}$	Infiltration capacity of non-compacted soil	mm t^{-1}	infiltpsoil	100.0 mm day^{-1}
$c_{infiltration, paved}$	Infiltration capacity of compacted soil	mm t^{-1}	infiltpcpath	10.0 mm day^{-1}
$z_{rooting}$	Rooting depth	mm	rootingdepth	750.0
$\frac{E_{gash}}{P_{sat}}$	Gash interception model parameter	-	e_r	0.1
LAI	Leaf area index	-	leaf_area_index	-
S_{leaf}	Specific leaf storage	mm	sl	-
$S_{canopy, max}$	Canopy storage capacity	mm	cmax	1.0
$f_{canopygap}$	Canopy gap fraction	-	canopygapfraction	0.1
$S_{wood, max}$	Storage capacity woody parts of vegetation	mm	swood	-
k	Extinction coefficient	-	kext	-
c_{rd}	Model parameter controlling the sigmoid function, for the fraction of wet roots	-	rootdistpar	-500.0
$z_{cap, maxdepth}$	Critical water depth beyond which capillary rise ceases	mm	cap_hmax	2000.0
m	Empirical coefficient controlling capillary rise	-	cap_n	2.0
K_{v0}	Vertical saturated hydraulic conductivity at the soil surface	mm t^{-1}	kv0	3000.0 mm day^{-1}
f_{Kv}	Scaling parameter for saturated hydraulic conductivity	mm $^{-1}$	f	0.001
c_n	Brooks-Corey power coefficient	-	c	10.0
h_b	Air entry value	cm	hb	10.0
L_{max}	Maximum allowed leakage	mm t^{-1}	maxleakage	0.0 mm day^{-1}
f_{Kl0}	Multiplication factor applied to K_{v0} (for lateral subsurface flow)	-	-	1.0
$f_{Kv, n}$	Multiplication factor (correcting vertical hydraulic conductivity)	-	kvfrac	1.0
s_{ddf}	Degree-day-melt factor snow	mm °C $^{-1} t^{-1}$	cfmax	3.75653 mm °C $^{-1} day^{-1}$
$s_{fall, Tthreshold}$	Temperature threshold for snowfall	°C	tt	0.0
$s_{fall, Tinterval}$	Temperature threshold interval for snowfall	°C	tti	1.0
$s_{melt, Tthreshold}$	Temperature threshold for snowmelt	°C	ttm	0.0
s_{whc}	Water holding capacity of snow	-	whc	0.1
$g_{melt, Tthreshold}$	Temperature threshold for glacier melt	°C	g_tt	0.0
g_{ddf}	Degree-day-melt factor glacier	mm °C $^{-1} t^{-1}$	g_cfmax	3.0 mm °C $^{-1} day^{-1}$
$f_{glacier}$	Fraction covered by a glacier	-	glacierfrac	0.0
$S_{glacier}$	Glacier storage	mm	glacierstore	5500.0
$g_{snow to ice}$	Fraction of snow that is converted into ice	-	g_sifrac	0.001
w	Weighting coefficient	-	w_soil	0.1125
$f_{red, frozen}$	Controlling infiltration reduction factor	-	cf_soil	0.038
$c_{land slope}$	Slope of the land surface	m m^{-1}	β_1	-
$c_{river slope}$	Slope of river	m m^{-1}	sl	-
A_{res}	Reservoir area	m 2	area	-
$Q_{min req.}$	Minimum flow requirement downstream of the reservoir	m $^3 s^{-1}$	demandrelease	-
$Q_{max, res}$	Maximum release capacity spillway	m $^3 s^{-1}$	maxrelease	-
$S_{res, max}$	Maximum storage of the reservoir	m 3	maxvolume	-
$f_{res, min}$	Target minimum storage fraction	-	targetminfrac	-
$f_{res, max}$	Target maximum storage fraction	-	targetmaxfrac	-
A_{lake}	Lake area	m 2	area	-
$H_{0, lake}$	Water level lake threshold below no outflow occurs	m	threshold	-
H_{lake}	Water level lake	m	waterlevel	-
β	Rating curve coefficient	-	b	-
α	Rating curve exponent	-	e	-
n_{land}	Manning's roughness (overland flow)	$c_{land slope} m^{-\frac{1}{3}}$	n	0.072
n_{river}	Manning's roughness (river flow)	$c_{river slope} m^{-\frac{1}{3}}$	n	0.036
x_{river}	River length	m	dl	-
w_{river}	River width	m	width	-
$h_{bankfull}$	River bankfull depth	m	bankfull_depth	1.0



References

- Aerts, J. P. M., Hut, R. W., van de Giesen, N. C., Drost, N., van Verseveld, W. J., Weerts, A. H., and Hazenberg, P.: Large-sample assessment of spatial scaling effects of the distributed wflow_sbm hydrological model shows that finer spatial resolution does not necessarily lead to better streamflow estimates, *Hydrol. Earth Syst. Sci. Discuss.* [preprint], <https://doi.org/10.5194/hess-2021-605>, in review, 2021.
- 850 Alfieri, L., Burek, P., Dutra, E., Krzeminski, B., Muraro, D., Thielen, J., and Pappenberger, F.: GloFAS – global ensemble streamflow forecasting and flood early warning, *Hydrol. Earth Syst. Sci.*, 17, 1161–1175, <https://doi.org/10.5194/hess-17-1161-2013>, 2013.
- Arino O., Ramos, J., Kalogirou, V., Defourny, P., and Achard., F.: GlobCover 2009, ESA Living Planet Symposium, 27 June, 2 July 2010, Bergen, Norway.
- Bell, V. A., Kay, A. L., Jones, R. G., and Moore, R. J.: Development of a high resolution grid-based river flow model for use with regional
855 climate model output, *Hydrol. Earth Syst. Sci.*, 11, 532–549, doi: 10.5194/hess-11-532-2007951, 2007.
- Benning, R. G.: Towards a new lumped parameterization at catchment scale (Doctoral dissertation, Wageningen University, Wageningen, The Netherlands). Retrieved from <http://edepot.wur.nl/216531ID954>, 1994.
- Bergström, S.: The HBV model – its structure and applications, SMHI Norrköping, Schweden, SMHI, SMHI Reports Hydrology, 4, 32 pp., 1992.
- 860 Bezanson, J., Edelman, A., Karpinski, S., and Shah, V. B.: Julia: A Fresh Approach to Numerical Computing, *SIAM Rev.*59, 1, 2017, <https://doi.org/10.1137/141000671>
- Beven, K.: Prophecy, reality, and uncertainty in distributed hydrological modeling, *Adv. Water Resour.*, 16, 41-51, 1993.
- Beven, K.: A manifesto for the equifinality thesis, *J. Hydrol.*, 320, 18-36, 2006.
- Bierkens, M. F. P., et al.: Hyper-resolution global hydrological modelling: What is next? “Everywhere and locally relevant”, *Hydrol. Processes*, 29, 310–320, 2014.
- 865 Brakensiek, D. L., Rawls, W. J., and Stephenson, G. R.: Modifying scs hydrologic soil groups and curve numbers for rangeland soils, ASAE Paper no. PNR-84-203, St. Joseph, Michigan, USA, 1984.
- Brooks, R. H., and Corey, A. T.: Hydraulic properties of porous media, *Hydrology Papers* 3, Colorado State University, Fort Collins, 27 p., 1964.
- 870 Brunner, P., and Simmons, C. T.: HydroGeoSphere: A Fully Integrated, Physically Based Hydrological Model, *Groundwater*, 50, 170-176, 2012.
- Buchhorn, M., Smets, B., Bertels, L., Lesiv, M., Tsendbazar, N.-E., Herold, M., and Fritz, S.: Copernicus Global Land Service: Land Cover 100m, epoch 2015, *Globe (Version V2.0.2)*, <http://doi.org/10.5281/zenodo.3243509>, 2019.
- Chow, V. T., Maidment, D. R., and Mays, L. W.: *Applied Hydrology*, McGraw-Hill International Editions, Civil Engineering Series, 1988.
- 875 Clark, M. P., et al.: Improving the theoretical underpinnings of processbased hydrologic models, *Water Resour. Res.*, 52, 2350–2365, doi:10.1002/2015WR017910, 2016.
- Clark, M. P., et al.: The evolution of process-based hydrologic models: historical challenges and the collective quest for physical realism, *Hydrol. Earth Syst. Sci.*, 21, 3427–3440, 2017.
- Cornelissen, T., Diekkrüger, B., Giertz, S.: A comparison of hydrological models for assessing the impact of land use and climate
880 change on discharge in a tropical catchment, *Journal of Hydrology*, Volume 498, 2013, Pages 221-236, ISSN 0022-1694, <https://doi.org/10.1016/j.jhydrol.2013.06.016>.



- de Bruin, H. A. R. d., Trigo, I. F., Bosveld, F. C., and Meirink, J. F.: A Thermodynamically Based Model for Actual Evapotranspiration of an Extensive Grass Field Close to FAO Reference, Suitable for Remote Sensing Application, *Journal of Hydrometeorology*, 17, 1373-1382, <https://doi.org/10.1175/JHM-D-15-0006.1>, publisher: American Meteorological Society Section: Journal of Hydrometeorology, 2016.
- 885 Eilander, D., and Boisgontier, H.: hydroMT (v0.4.5), Zenodo, <https://doi.org/10.5281/zenodo.610766>, 2022.
- Eilander, D., Boisgontier, H., van Verseveld, W., Bouaziz, L., and Hegnauer, M.: hydroMT-wflow (v0.1.4), Zenodo, <https://doi.org/10.5281/zenodo.6221375>, 2022.
- Eilander, D., van Verseveld, W., Yamazaki, D., Weerts, A., Winsemius, H. C., and Ward, P. J.: A hydrography upscaling method for scale-invariant parametrization of distributed hydrological models, *Hydrol. Earth Syst. Sci.*, 25, 5287–5313, <https://doi.org/10.5194/hess-25-5287-2021>, 2021.
- 890 Engman, E.: Roughness coefficients for routing surface runoff, *J. Irrig. Drain. Eng.*, 112, 39–53, doi: 10.1061/(ASCE)0733-9437(1986)112:1(39), 1986.
- ESDAC: The European Soil Database distribution version 2.0, European Commission and the European Soil Bureau Network, 2004. Retrieved from esdac.jrc.ec.europa.eu
- 895 European Environment Agency: Corine Land Cover (CLC) 2018, Version 2020_20u1, Retrieved from <https://land.copernicus.eu/pan-european/corine-land-cover/clc2018>, 2018.
- Fan, J., McConkey, B., Wang, H., and Janzen, H.: Root distribution by depth for temperate agricultural crops, *Field Crops Res.*, 189, 68-74, <https://doi.org/10.1016/j.fcr.2016.02.013>, 2016.
- Feddes, R.A., Kowalik, P.J. and Zaradny, H.: Simulation of field water use and crop yield, Pudoc, Wageningen, Simulation Monographs, 900 1978.
- Feigl, M., Herrnegger, M., Klotz, D., and Schulz, K.: Function space optimization: A symbolic regression method for estimating parameter transfer functions for hydrological models, *Water Resources Research*, 56, e2020WR027385. <https://doi.org/10.1029/2020WR027385>, 2020.
- Fenicia, F., Kavetski, D., and Savenije, H. H.: Elements of a flexible approach for conceptual hydrological modeling: 1. Motivation and theoretical development, *Water Resour. Res.*, 47, W11510, <https://doi.org/10.1029/2010WR010174>, 2011.
- 905 Funk, C., Peterson, P., Landsfeld, M. et al.: The climate hazards infrared precipitation with stations—a new environmental record for monitoring extremes, *Sci Data* 2, 150066, <https://doi.org/10.1038/sdata.2015.66>, 2015.
- Gao, H., Hrachowitz, M., Fenicia, F., Gharari, S., and Savenije, H. H. G.: Testing the realism of a topography-driven model (FLEX-Topo) in the nested catchments of the Upper Heihe, China, *Hydrol. Earth Syst. Sci.*, 18, 1895–1915, <https://doi.org/10.5194/hess-18-1895-2014>, 910 2014.
- Gash, J. H. C.: An analytical model of rainfall interception by forests, *Q. J. Roy. Meteor. Soc.*, 105, 43–55, doi:10.1002/qj.497105443041027, 1979.
- Gebremicael, T., Mohamed, Y., and der Zaag, P.V.: Attributing the hydrological impact of different land use types and their long-term dynamics through combining parsimonious hydrological modelling, alteration analysis and PLSR analysis, *Sci. Total Environ.*, 660, pp. 1155-1167, [10.1016/j.scitotenv.2019.01.085](https://doi.org/10.1016/j.scitotenv.2019.01.085), 2019.
- 915 Giardino, A., Schrijvershof, R., Nederhoff, C., De Vroeg, H., Brière, C., Tonnon, P.K., Caires, S., Walstra, D., Sosa, J., Van Verseveld, W., Schellekens, J., and Sloff, C. J.: A quantitative assessment of human interventions and climate change on the West African sediment budget, *Ocean Coast. Manag.*, 156, 249–265, <https://doi.org/10.1016/j.ocecoaman.2017.11.008>, 2018.



- Gupta, H., Kling, H., Yilmaz, K., and Martinez, G.: Decomposition of the mean squared error and nse performance criteria: Implications for
920 improving hydrological modelling, *J. Hydr.*, 377, 80–91. doi:10.1016/j.jhydrol.2009.08.0031037, 2009.
- Hassaballah, K., Mohamed, Y., Uhlenbrook, S., and Biro, K.: Analysis of streamflow response to land use and land cover changes using
satellite data and hydrological modelling: case study of Dinder and Rahad tributaries of the Blue Nile (Ethiopia-Sudan). *Hydrol. Earth
Syst. Sci.* 21, 5217, <https://doi.org/10.5194/hess-21-5217-2017>, 2017.
- Hengl, T., Mendes de Jesus, J., Heuvelink, G. B. M., Ruiperez Gonzalez, M., Kilibarda, M., Blagotić, A., et al.: SoilGrids250m: Global
925 gridded soil information based on machine learning, *PLoS ONE*, 12, <https://doi.org/10.1371/journal.pone.0169748>, 2017.
- Hersbach, H., Bell, B., Berrisford, P., Hirahara, S., Horányi, A., Muñoz-Sabater, J., Nicolas, J., Peubey, C., Radu, R., Schepers, D., Simmons,
A., Soci, C., Abdalla, S., Abellan, X., Balsamo, G., Bechtold, P., Biavati, G., Bidlot, J., Bonavita, M., De Chiara, G., Dahlgren, P., Dee,
D., Diamantakis, M., Dragani, R., Flemming, J., Forbes, R., Fuentes, M., Geer, A., Haimberger, L., Healy, S., Hogan, R. J., Hólm, E.,
Janisková, M., Keeley, S., Laloyaux, P., Lopez, P., Lupu, C., Radnoti, G., de Rosnay, P., Rozum, I., Vamborg, F., Villaume, S., and Thépaut,
930 J.-N.: The ERA5 global reanalysis, *Q. J. Roy. Meteor. Soc.*, 146, 1999–2049, <https://doi.org/10.1002/qj.3803>, 2020.
- Horn, B. K. P.: Hill Shading and the Reflectance Map, *Proceedings of IEEE*, Vol. 69, No. 1, 1981, pp. 14-47, 1981,
<http://dx.doi.org/10.1109/PROC.1981.11918>
- Hrachowitz, M., and Clark M. P.: HESS Opinions: The complementary merits of competing modelling philosophies in hydrology, *Hydrol.
Earth Syst. Sci.*, 21, 3953–3973, <https://doi.org/10.5194/hess-21-3953-2017>, 2017.
- 935 Imhoff, R. O., van Verseveld, W. J., Osnabrugge, B., and Weerts, A. H.: Scaling Point-Scale (Pedo)transfer Functions to Seamless Large-
Domain Parameter Estimates for High-Resolution Distributed Hydrologic Modeling: An Example for the Rhine River, *Water Resour. Res.*,
56, <https://doi.org/10.1029/2019WR026807>, 2020.
- Jägermeyr, J., Pastor, A., Biemans, H., and Gerten, D.: Reconciling irrigated food production with environmental flows for Sustainable
Development Goals implementation, *Nat. Commun.* 8, 15900 doi: 10.1038/ncomms15900, 2017.
- 940 Jakeman, A. J., and Hornberger, G. M.: How Much Complexity Is Warranted in a Rainfall-Runoff Model?, *Water Resour. Res.*, 29, 2637-
2649, 1993.
- Karssenberg, D., Schmitz, O., Salamon, P., de Jong, K., and Bierkens, M. F. P.: A software framework for construction of process-based
stochastic spatio-temporal models and data assimilation, *Environ. Modell. Softw.*, 25, 489–502. doi: 10.1016/j.envsoft.2009.10.0041062,
2010.
- 945 Kilgore, J. L.: Development and evaluation of a gis-based spatially distributed unit hydrograph model, MSc. thesis, Retrieved from
<http://hdl.handle.net/10919/35777>, 1997.
- Kirchner, J. W.: Getting the right answers for the right reasons: Linking measurements, analyses, and models to advance the science of
hydrology, *Water Resour. Res.*, 42, W03S04, doi:10.1029/2005WR004362. 2006.
- Kling, H., Fuchs, M. and Paulin, M.: Runoff conditions in the upper Danube basin under an ensemble of climate change scenarios, *J. Hydrol.*,
950 424-425, 264–277, doi:10.1016/j.jhydrol.2012.01.011, 2012.
- Knoben, W. J. M., Clark, M. P., Bales, J., Bennett, A., Gharari, S., Marsh, C. B., Nijssen, B., Pietroniro, A., Spiteri, R. J., Tarboton,
D. G., and Wood, A. W.: Community Workflows to Advance Reproducibility in Hydrologic Modeling: Separating model-agnostic
and model-specific configuration steps in applications of large-domain hydrologic models, *Earth and Space Science Open Archive*,
<https://doi.org/10.1002/essoar.10509195.1>, 2021.
- 955 Knoben, W. J. M., Freer, J. E., and Woods, R. A.: Technical note: Inherent benchmark or not? Comparing Nash–Sutcliffe and Kling–Gupta
efficiency scores, *Hydrol. Earth Syst. Sci.*, 23, 4323–4331, <https://doi.org/10.5194/hess-23-4323-2019>, 2019.



- Kollet, S. J., and R. M. Maxwell; Integrated surface groundwater flow modeling: A free surface overland flow boundary condition in a parallel groundwater flow model, *Adv. Water Resour.*, 29, 945–958, doi:10.1016/j.advwatres.2005.08.006, 2006.
- 960 Laverde-Barajas, M., Corzo Perez, G. A., Chishtie, F., Poortinga, A., Uijlenhoet, R., and Solomatine, D. P.: Decomposing satellite-based rainfall errors in flood estimation: Hydrological responses using a spatiotemporal object-based verification method, *Journal of Hydrology*, Volume 591, 125554, ISSN 0022-1694, <https://doi.org/10.1016/j.jhydrol.2020.125554>, 2020.
- Lehner, B., Reidy Liermann, C., Revenga, C., Vörösmarty, C., Fekete, B., Cruzet, P., Döll, P., Endejan, M., Frenken, K., Magome, J., Nilsson C., Robertson, J. C., Rodel, R., Sindorf, N., and Wisser, D.: High-Resolution Mapping of the World's Reservoirs and Dams for Sustainable River- Flow Management, *Front. Ecol. Environ.*, 9, 494-502, <http://dx.doi.org/10.1890/100125>, 2011.
- 965 Lin, P., Pan, M., Allen, G., Frasson, R., Zeng, Z., Yamazaki, D., and Wood, E.: Global estimates of reach-level bankfull river width leveraging big-data geospatial analysis [Data set], Zenodo, <https://doi.org/10.5281/zenodo.3552776>, 2019.
- Liu, S.: Estimation of rainfall storage capacity in the canopies of cypress wetlands and slash pine uplands in North-Central Florida, *J. Hydr.*, 207, 32–41, doi: 10.1016/S0022-1694(98)00115-2, 1998.
- Liu, Z., Martina, M. L. V., and Todini, E.: Flood forecasting using a fully distributed model: application of the TOPKAPI model to the Upper
970 Xixian Catchment, *Hydrol. Earth Syst. Sci.*, 9, 347–364, doi: 10.5194/hess-9-347-2005, 2005.
- López López, P., Wanders, N., Schellekens, J., Renzullo, L. J., Sutanudjaja, E. H., and Bierkens, M. F. P.: Improved large-scale hydrological modelling through the assimilation of streamflow and downscaled satellite soil moisture observations, *Hydrol. Earth Syst. Sci.*, 20, 3059–3076, <https://doi.org/10.5194/hess-20-3059-2016>, 2016.
- Maurer, E., Wood, A., Adam, J., Lettenmaier, D., and Nijssen, B.: A long-term hydrologically based dataset of land
975 surface fluxes and states for the conterminous United States, *J. Climate*, 15, 3237–3251, [https://doi.org/10.1175/1520-0442\(2002\)015<3237:ALTHBD>2.0.CO;2](https://doi.org/10.1175/1520-0442(2002)015<3237:ALTHBD>2.0.CO;2), 2002.
- Meijer, K., Verschelling, E., van Verseveld, W., Donchyts, G., Schmeier, S., and Kwadijk, J.: Fit for purpose? Rapid development of water allocation models using global data: Application for the Upper Niger Basin, *Environmental Modelling & Software*, Volume 145, 105168, ISSN 1364-8152, <https://doi.org/10.1016/j.envsoft.2021.105168>, 2021.
- 980 Melsen, L. A., Teuling, A. J., Torfs, P. J. J. F., and Clark, M. P.: HESS Opinions: The need for process-based evaluation of large-domain hyper-resolution models, *Hydrol. Earth Syst. Sci.*, 20, 1069–1079, doi: 10.5194/hess-20-1069-2016, 2016.
- Messenger, M.L., Lehner, B., Grill, G., Nedeva, I., and Schmitt, O.: Estimating the volume and age of water stored in global lakes using a geo-statistical approach, *Nat. Commun.*, 7, <https://doi.org/10.1038/ncomms13603>, 2016.
- Mizukami, N., Clark, M. P., Gharari, S., Kluzek, E., Pan, M., Lin, P., et al.: A vector-based river routing model for Earth Sys-
985 tem Models: Parallelization and global applications, *Journal of Advances in Modeling Earth Systems*, 13, e2020MS002434. <https://doi.org/10.1029/2020MS002434>, 2021.
- Myneni, R. B., Knyazikhin, Y., and Park, T.: MCD15A3H MODIS/Terra+Aqua Leaf Area Index/FPAR 4-day L4 Global 500m SIN Grid V006 (Tech. Rep.): NASA EOSDIS and Pocesess DAAC, 2015.
- Neal, J., Schumann, G., and Bates P.: A subgrid channel model for simulating river hydraulics and floodplain inundation over large and data
990 sparse areas, *Water Resour. Res.*, 48, W11506, doi:10.1029/2012WR012514, 2012.
- O’Neill, P. E., S. Chan, E. G. Njoku, T. Jackson, R. Bindlish, J. Chaubell, and Colliander, A.: SMAP Enhanced L3 Radiometer Global and Polar Grid Daily 9 km EASE-Grid Soil Moisture, Version 5. [53°N, 12°W; 45°N, 3°W]. Boulder, Colorado USA. NASA National Snow and Ice Data Center Distributed Active Archive Center. doi: <https://doi.org/10.5067/4DQ54OUIJ9DL>. [01-11-2022].



- Pekel, J. F., Cottam, A., Gorelick, N., and Belward, A. S.: High resolution mapping of global surface water and its long term changes, *Nature*, 995 540, 418–422, <https://doi.org/10.1038/nature20584>, 2016.
- Pfeffer, W. T., Arendt, A. A., Bliss, A., Bolch, T., Cogley, J. G., Gardner, A. S., Hagen, J.-O., Hock, R., Kaser, G., Kienholz, C., Miles, 510 E. S., Moholdt, G., Mölg, N., Paul, F., Radic, V., Rastner, P., Raup, B. H., Rich, J., Sharp, M. J., and Consortium, T. R.: The Randolph Glacier Inventory: a globally complete inventory of glaciers, *Journal of Glaciology*, 60, 537–552, <https://doi.org/10.3189/2014JoG13J176>, publisher: Cambridge University Press, 2014.
- 1000 Pitman, J.: Rainfall interception by bracken in open habitats—relations between leaf area, canopy storage and drainage rate, *J. Hydr.*, 105, 317–334, doi: 10.1016/0022-1694(89)90111-X, 1989.
- Rawls, W. J., and Brakensiek, D. L.: Estimation of Soil Water Retention and Hydraulic Properties, In H. J. Morel-Seytoux (Ed.), *Unsaturated flow in hydrologic modelling - Theory and practice*, NATO ASI Series 9, 275–300, Dordrecht, The Netherlands: Kluwer Academic Publishing, 1989.
- 1005 Rusli, S.R., Weerts, A.H., Taufiq, A., and Bense, V.F.: Estimating water balance components and their uncertainty bounds in highly groundwater-dependent and data-scarce area: An example for the Upper Citarum basin, *Journal of Hydrology: Regional Studies*, Volume 37, 2021, 100911, ISSN 2214-5818, <https://doi.org/10.1016/j.ejrh.2021.100911>.
- Rutter, A., Kershaw, K., Robins, P., and Morton, A.: A predictive model of rainfall interception in forests. 1. Derivation of the model from observations in a plantation of Corsican pine *Agric. Meteorol.*, 9, pp. 367–384, 10.1016/0002-1571(71)90034-3, 1971.
- 1010 Rutter, A., Morton, A., and Robins, P.: A predictive model of rainfall interception in forests. II. Generalization of the model and comparison with observations in some coniferous and hardwood stands *J. Appl. Ecol.*, pp. 367–380, 10.2307/2401739, 1975
- Samaniego, L., Kumar, R., and Attinger, S.: Multiscale parameter regionalization of a grid-based hydrologic model at the mesoscale, *Water Resour. Res.*, 46, doi: 10.1029/2008WR0073271178, 2010.
- Samaniego, L., Kumar, R., Thober, S., Rakovec, O., Zink, M., Wanders, N., Eisner, S., Müller Schmied, H., Sutanudjaja, E. H., Warrach- 1015 Sagi, K., and Attinger, S.: Toward seamless hydrologic predictions across spatial scales, *Hydrol. Earth Syst. Sci.*, 21, 4323–4346, <https://doi.org/10.5194/hess-21-4323-2017>, 2017.
- Schellekens, J., van Verseveld, W., Visser, M., Winsemius, H., Bouaziz, L., Euser, T., De Vries, S., Thiange, C., Boisgontier, H., Eilander, D., Tollenaar, D., Weerts, A., Baart, F., Hazenberg, P., Pronk, M., Lutz, A., Ten Velden, C., Benedict, I., and Jansen, M.: *openstreams/wflow: Bug fixes and updates for release 2020.1.2*, <https://zenodo.org/record/4291730>.
- 1020 Schenk, H. J., and Jackson, R. B.: The global biogeography of roots. *Ecological monographs*, 72, 311–328, [https://doi.org/10.1890/0012-9615\(2002\)072\[0311:TGBOR\]2.0.CO;2](https://doi.org/10.1890/0012-9615(2002)072[0311:TGBOR]2.0.CO;2), 2002.
- Seibert, J., Vis, M. J. P., Kohn, I., Weiler, M., and Stahl, K.: Technical note: Representing glacier geometry changes in a semi-distributed hydrological model, *Hydrol. Earth Syst. Sci.*, 22, 2211–2224, <https://doi.org/10.5194/hess-22-2211-2018>, 2018.
- Séguis, L., Kamagaté, B., Favreau, G., Descloitres, M., Seidel, J.-L., Galle, S., Peugeot, C., Gosset, M., Le Barbé, L., Malinur, F., Van Exter, 1025 S., Arjounin, M., Boubkraoui, S., Wubda, M.: Origins of streamflow in a crystalline basement catchment in a sub-humid Sudanian zone: The Donga basin (Benin, West Africa): Inter-annual variability of water budget, *Journal of Hydrology*, Volume 402, Issues 1–2, 2011, Pages 1–13, ISSN 0022-1694, <https://doi.org/10.1016/j.jhydrol.2011.01.054>.
- Šimůnek, J., van Genuchten, M. T., and Šejna, M.: Development and applications of the HYDRUS and STANMOD software packages and related codes, *Vadose Zone J.*, 7, 587–600, 2008.
- 1030 <https://vattenwebb.smhi.se/station/>, last access: 25 January 2021.



- Swedish Meteorological and Hydrological Institute: Model Performance Europe, [online] Available from: <https://hypeweb.smhi.se/explore-water/model-performances/model-performance-europe/> (Accessed 2 June 2022), 2022.
- Sperna Weiland, F.C., Visser, R.D., Greve, P., Bisselink, B., Brunner, L., and Weerts, A.H.: Estimating Regionalized Hydrological Impacts of Climate Change Over Europe by Performance-Based Weighting of CORDEX Projections, *Frontiers of Water*, 10.3389/frwa.2021.713537, 2021.
- Tanaka, T., and Tachikawa, Y.: Testing the applicability of a kinematic wave-based distributed hydrologic model in two climatically contrasting catchments, *Hydrolog. Sci. J.*, 60, 1361–1373, <https://doi.org/10.1080/02626667.2014.967693>, 2015.
- Todini, E., and Ciarapica, L.: Mathematical models of large watershed hydrology. In V. P. Singh and D. K. Frevert (Eds.), (pp. 471–506). Water Resources Publications, Littleton, Colorado, 2002.
- Tóth, B., Weynants, M., Nemes, A., Makó, A., Bilas, G., and Tóth, G.: New generation of hydraulic pedotransfer functions for Europe, *Eur. J. Soil Sci.*, 66, 226–238. doi: 10.1111/ejss.121921211, 2015.
- Trambauer, P., Werner, M., Winsemius, H. C., Maskey, S., Dutra, E., and Uhlenbrook, S.: Hydrological drought forecasting and skill assessment for the Limpopo River basin, southern Africa, *Hydrol. Earth Syst. Sci.*, 19, 1695–1711, <https://doi.org/10.5194/hess-19-1695-2015>, 2015.
- van Beek, L. P. H., Wada, Y., and Bierkens, M. F. P.: Global monthly water stress: 1. Water balance and water availability, *Water Resour. Res.*, 47, W07517, doi:10.1029/2010WR009791, 2011.
- Van Dijk, A. I. J. M., and Bruijnzeel, L. A.: Modelling rainfall interception by vegetation of variable density using an adapted analytical model, Part 2, Model validation for a tropical upland mixed cropping system, *J. Hydr.*, 247, 239–262. 2001.
- Van Looy, K., Bouma, J., Herbst, M., Koestel, J., Minasny, B., Mishra, U., Vereecken, H.: Pedotransfer functions in Earth system science: Challenges and perspectives, *Rev. Geophys.*, 55, 1199–1256, <https://doi.org/10.1002/2017RG000581>, 2017.
- van Verseveld, W., Visser, M., Boisgontier, H., Bootsma, H., Bouaziz, L., Buitink, J., Eilander, D., and Hegnauer, M.: Wflow_jl (v0.6.1), Zenodo, <https://doi.org/10.5281/zenodo.6490936>, 2022a.
- van Verseveld, W., Weerts, A., and Imhoff, R.: Wflow_sbm v0.6.1 model cases (0.1), [Data set], Zenodo, <https://doi.org/10.5281/zenodo.6821468>, 2022b.
- Vertessy, R., and Elsenbeer, H.: Distributed modeling of storm flow generation in an amazonian rain forest catchment: effects of model parameterization, *Water Resour. Res.*, 35, 2173–2187. doi: 10.1029/1999WR9000511257, 1999.
- Yamazaki, D., Ikeshima, D., Sosa, J., Bates, P. D., Allen, G. H., and Pavelsky, T. M.: MERIT Hydro: a high resolution global hydrography map based on latest topography dataset, *Water Resour. Res.*, 55, 5053–5073, <https://doi.org/10.1029/2019WR024873>, 2019.
- Yamazaki, D., Ikeshima, D., Tawatari, R., Yamaguchi, T., O’Loughlin, F., Neal, J. C., Sampson, C. C., Kanae, S., and Bates, P. D.: A high accuracy map of global terrain elevations, *Geophys. Res. Lett.*, 44, 5844–5853. <https://doi.org/10.1002/2017GL072874>, 2017.
- Yamazaki, D., Trigg, M. A., and Ikeshima, D.: Development of a global 90 m water body map using multitemporal Landsat images, *Remote Sens. Environ.*, 171, 337–351. <https://doi.org/10.1016/j.rse.2015.10.014>, 2015.
- Yang, F., Zhang, G., Yin, X., Liu, Z., and Huang, Z.: Study on capillary rise from shallow groundwater and critical water table depth of a saline-sodic soil in western Songnen plain of China, *Environ. Earth Sci.* 64, 2119–2126, <https://doi.org/10.1007/s12665-011-1038-4>, 2011.
- Wang, X., Huo, Z., Feng, S., Guo, P., and Guan, H.: Estimating groundwater evapotranspiration from irrigated cropland incorporating root zone soil texture and moisture dynamics, *Journal of Hydrology*, 543, 501–509, <https://doi.org/10.1016/j.jhydrol.2016.10.027>, 2016.f



- 1070 Wannasin, C., Brauer, C., Uijlenhoet, R., van Verseveld, W., and Weerts, A.: Daily flow simulation in thailand part I: testing a distributed hydrological model with seamless parameter maps based on global data, *J. Hydrol.: Reg. Stud.*, 34, p. 100794, 10.1016/j.ejrh.2021.100794, 2021a.
- Wannasin, C., Brauer, C., Uijlenhoet, R., van Verseveld, W., and Weerts, A.: Daily flow simulation in thailand part II: unraveling effects of reservoir operation, *J. Hydrol.: Reg. Stud.*, 34, p. 100792, 10.1016/j.ejrh.2021.100792, 2021b.
- Wigmosta, M. S., Lane, L. J., Tagestad, J. D., and Coleman A. M.: Hydrologic and erosion models to assess land use and management practices affecting soil erosion, *J. Hydrol. Eng.*, 14, 27-41, 2009.
- 1075 Wood, E. F., et al.: Hyperresolution global land surface modeling: Meeting a grand challenge for monitoring Earth's terrestrial water, *Water Resour. Res.*, 47, W05301, doi:10.1029/2010WR010090, 2011.
- Zammouri, M.: Case study of water table evaporation at Ichkeul Marshes (Tunisia). *J. Irrig. Drain. Eng.* 127, 265–271, 2001.
- Zhao, F., Veldkamp, T. I. E., Frieler, K., Schewe, J., Ostberg, S., Willner, S., Schauburger, B., Gosling, S. N., Schmied, H. M., Portmann, F. T., Leng, G., Huang, M., Liu, X., Tang, Q., Hanasaki, N., Biemans, H., Gerten, D., Satoh, Y., Pokhrel, Y., Yamazaki, D.: The critical role
1080 of the routing scheme in simulating peak river discharge in global hydrological models, *Environmental Research Letters*, 12(7), 075003. <https://doi.org/10.1088/1748-9326/aa7250>, 2017.